Journal of Food Composition and Analysis 144 (2025) 107702

Contents lists available at ScienceDirect

Journal of Food Composition and Analysis

journal homepage: www.elsevier.com/locate/jfca

A highly selective electrochemical sensor by using bimetallic metal organic framework for the detection of 3-Monochloropropane-1,2-diol esters (3-MCPDEs)

Sharifah Shahira Syed Putra [a,b,1], Md. Shalauddin [c,*,1], Shamima Akhter [d,*], Wan Jefrey Basirun [e,f,*], Amal A.M. Elgharbawy [g], Syed Rahin Ahmed [h], Seshasai Srinivasan [h,*], Amin Reza Rajabzadeh [h,**], Adeeb Hayyan [b], Yousef Mohammed Alanazi [i], Barun Kumar Chakrabarti [j], Chee Tong John Low [k]

[a] Faculty of Industrial Sciences and Technology, Universiti Malaysia Pahang Al-sultan Abdullah, Lebuhraya Tun Abdul Razak, Gambang, Pahang 26300, Malaysia
[b] Department of Chemical Engineering, Faculty of Engineering, Universiti Malaya, Kuala Lumpur 50603, Malaysia
[c] School of Pharmacy, Faculty of Health and Medical Sciences, Taylor's University, Subang Jaya, Selangor 47500, Malaysia
[d] Department of Pharmaceutical Chemistry, School of Pharmacy, IMU University, Bukit Jalil, Kuala Lumpur 57000, Malaysia
[e] Nanotechnology and Catalysis Research Center (NANOCAT), Universiti Malaya, Kuala Lumpur 50603, Malaysia
[f] Department of Chemistry, Faculty of Science, Universiti Malaya, Kuala Lumpur 50603, Malaysia
[g] International Institute for Halal Research and Training (INHART), International Islamic University Malaysia, P.O Box 10, Kuala Lumpur 50728, Malaysia
[h] School of Engineering Practice & Technology, McMaster University, Hamilton, Ontario L8S 4L8, Canada
[i] Chemical Engineering Department, King Saud University, P.O. Box 800, Riyadh 11421, Saudi Arabia
[j] Sabanci University Nanotechnology Research and Application Centre (SUNUM), Orta Mah. Üniversite Cad. No: 27/1, İstanbul, Tuzla 34956, Turkey
[k] WMG, Warwick Electrochemical Engineering Group, Energy Innovation Centre, University of Warwick, Coventry CV4 7AL, United Kingdom

ARTICLE INFO

Keywords:
3-chloro-1
2-propanediol esters
Metal-organic framework
Cyclic voltammetry
Electrochemical impedance spectroscopy
Square wave voltammetry

ABSTRACT

3-Monochloropropane-1,2-diol esters (3-MCPDEs) are hazardous contaminants in heat-processed foods, raising serious food safety concerns. In this study, a high-performance Fe-Mn-MOF/NIF sensor was developed via a simple hydrothermal method for rapid and precise 3-MCPDEs detection. Structural and morphological analyses confirmed the sensor stability, with FTIR revealing strong interactions between (-CH) and (O-H) stretching vibrations, while XRD indicated slight crystal distortion upon detection. FESEM and TEM confirmed minimal aggregation, ensuring homogeneous iron (Fe) and manganese (Mn) distribution. The sensor exhibited a large surface area, significantly enhancing its detection capability. Using square wave voltammetry (SWV) method, it achieved a broad linear range (0.05–255 μM), low detection limit (0.002 μM), and exceptional sensitivity (43.71 μA μM^{-1} cm^{-2}). Comparative analysis with GC-MS demonstrated comparable accuracy, while real-sample testing in soy sauce confirmed high recovery rates. Unlike conventional methods, this sensor enables cost-effective, rapid, and on-site detection, offering a transformative approach for food safety monitoring. With its superior performance, the Fe-Mn-MOF/NIF sensor presents a breakthrough in electrochemical detection, paving the way for enhanced food quality control and public health protection.

1. Introduction

3-MCPDEs, a by-product formed during the process of fatty acid deformation, is one of the most common food contaminants (Ahn et al., 2020). In other words, 3-MCPDEs are the esterified forms of 3-MCPD, predominantly found in processed vegetable oils, including palm oil. During digestion, 3-MCPDEs break down, releasing free 3-MCPD, thereby posing a similar toxicological risk. These compounds are

* Corresponding authors.
** Corresponding author at: Nanotechnology and Catalysis Research Center (NANOCAT), Universiti Malaya, Kuala Lumpur 50603, Malaysia.
E-mail addresses: md.shalauddin@taylors.edu.my (Md. Shalauddin), shamimaakhter@imu.edu.my (S. Akhter), jeff@um.edu.my (W.J. Basirun), ssriniv@mcmaster.ca (S. Srinivasan), rajaba@mcmaster.ca (A.R. Rajabzadeh).
[1] These authors contribute equally in this work.

https://doi.org/10.1016/j.jfca.2025.107702
Received 4 December 2024; Received in revised form 13 March 2025; Accepted 26 April 2025
Available online 28 April 2025

primarily produced when acylglycerols undergo deodorization at elevated temperatures in the presence of chlorinated compounds (JECFA, 2017). The presence of 3-MCPDEs has been observed in food products such as infant milk formula, soy sauce, and cheese due to industrial and domestic processing (Putra et al., 2022). The levels of esterified 3-MCPD also known as bound 3-MCPD, in refined oils and fats are around less than 0.03 parts per million (ppm) to 19 ppm (Araujo et al., 2020). Comprehensive toxicological studies show that 3-MCPDEs break down completely in the gastrointestinal tract due to the lipase action which releases the free 3-MCPD, causing toxic effects *in vivo* (Liu et al., 2021). The intake of 3-MCPD causes adverse effects on the kidneys and heart, weakens neurological functions, induces testicular damage and elevates the risk of certain types of cancers (Putra et al., 2023). The kidney is the primary target organ for 3-MCPD toxicity (Schultrich et al., 2020), and so a regulation for consumption and sensitive detection technique for 3-MCPD is needed.

European Union has set a regulatory intake limit of 3-MCPD of 0.02 mg/kg body weight per day for hydrolyzed vegetable protein and soy sauce (Arris et al., 2022). To date, several analytical techniques have been utilized for the detection of 3-MCPD in previous reports. These methods include the combination of gas chromatography and mass spectrometry (GC–MS) (Putra et al., 2023), gas chromatography-triple quadrupole mass spectrometry (Genualdi et al., 2017) and high-performance liquid chromatography with fluorescence detection (HPLC-FLD) (Dua et al., 2021). However, LOD for 3-MCPDEs remains relatively low due to its small molecular weight. Moreover, these methods often necessitate costly equipments and time-consuming experimental procedures (Han et al., 2021). Besides this, a range of nanomaterials such as graphene oxide (GO) (Yaman et al., 2021), graphite zero-valent iron (Arris et al., 2021), and perovskite (Zhao et al., 2021) has been utilized as a platform for 3-MCPD detection via electrochemical analysis. For instance, a conductive electrode for the detection of 3-MCPD was demonstrated by Arris et al. (2022) using a graphene-based acrylonitrile butadiene styrene (ABS) filament. Martin et al. (2021) fabricated a sensor by modifying a gold (Au) electrode with cysteine (Cys)-coated silver nanoparticles (Cys-AgNPs) for the detection of 3-MCPD in smoked mackerel and palm oil samples. Amino silica modified with fluorescein isothiocyanate (FITC) was utilized recently by Xu et al. (2023) for rapid fluorescence detection of 3-MCPD. Compared to other techniques, the electrochemical detection method offers faster response and make it portable for on-site monitoring. However, overcoming the matrix interference effectively while maintaining the sensitivity remains a significant challenge in electrochemical method of detection of 3-MCPDEs in food products (Cheng et al., 2022).

Therefore, metal organic frameworks (MOFs) have received significant attention for the detection of food contamination due to their larger surface area, high porosity, and adsorbent nature. Up-to-now, various types of synthesized MOFs have been studied for the detection of 3-MCPDEs in food products. For example, He et al. (2020) deposited gold-silver nanostars (Au@AgNSs) onto a gold electrode (AuE) coated with Fe-based metal-organic frameworks (Fe-MOF) for the detection of 3-MCPD in soy sauce. Meanwhile, Han et al. (2021) prepared carboxylated multi-wall carbon nanotubes (cMWCNT) incorporated in MOF with a low linear range of 1.2×10^{-5} to 0.12 mg/kg. Yet, the intricate synthesis process of the MOFs sensor and the necessity for repeated applications limit its scope of use in real life (Sun et al., 2023). In response to the limitations of existing MOFs sensors, bimetallic MOFs can be utilized for the detection of 3-MCPDEs in food products. The bimetallic MOFs possess notable characteristics such as a large specific surface area and well-organized pore structure, making them highly suitable for various applications such as catalysis, sensors, gas separation and storage (Sohouli et al., 2020). In comparison to conventional porous inorganic materials, bimetallic MOFs require moderate synthesis conditions with adaptable structure, allowing easier modifications (Amini et al., 2020). In particular, MOF based on iron (III) chloride (Fe-MOFs) or nanomaterials derived from Fe-MOFs demonstrate remarkable stability and impressive sensing capabilities when employed as electrode materials (Wang et al., 2019). Moreover, MOF based on manganese (III) chloride (Mn-MOF) exhibits robust stability in aqueous solutions, substantial porosity, outstanding biocompatibility and a distinct specific surface area as reported by Song et al. (2019).

Herein, this study presents a novel Fe-Mn-MOF/NIF electrochemical sensor for the highly sensitive detection of 3-MCPD. It integrates a bimetallic Fe-Mn MOF onto nickel foam (NIF), which serves as a conductive and porous substrate. This is the first time this approach has been used, employing the square wave voltammetry (SWV) method. Furthermore, this approach highlights a rapid and on-site detection, making it a promising alternative for real-time food safety monitoring. The practical applicability of the sensor was successfully validated using real soy sauce samples, achieving outstanding recovery rates. Given its high selectivity, minimal sample preparation, and superior analytical performance, this Fe-Mn-MOF/NIF sensor represents a transformative advancement in food contaminant detection, offering an efficient and scalable alternative to conventional laboratory-based techniques.

2. Materials and methods

2.1. Chemicals and reagents

Commercially available extra virgin olive (EVO) oil (Basso) was purchased from local supermarket. High purity (>98 %) rac 1,2-*bis*-palmitoyl-3-chloropropanediol (3-MCPDE) and the internal standard deuterated rac 1,2-*bis*-palmitoyl-3-chloropropanediol-d_5 (3-MCPDE-d_5) were purchased from Toronto Research Chemicals Inc. (Toronto, Canada). Dimethylformamide, 98 % terephthalic acid (TPA), 98 % iron (III) chloride ($FeCl_3$), 98 % manganese (III) chloride ($MnCl_3$) and ethanol were of analytical grade and purchased from Sigma-Aldrich. Ultrapure water was used for all synthesis and analytical procedures.

2.2. Instrumentation characterizations

The Fe-Mn-MOF/NIF sensor was characterized by the following instrumentation. Fourier-transformed infrared (FTIR) analysis (Shimadzu™ Corporation, Japan) was utilized to study the functional groups in the Fe-Mn-MOF/NIF nanocomposite. The crystal size and crystal structure of the synthesized nanocomposite were determined by an X-ray diffractometer (XRD) (Rigaku, Japan). The morphology of the synthesized MOF nanocomposites (Fe-MOF, Mn-MOF, and Fe-Mn-MOF/NIF) were analyzed by a field emission scanning electron microscope (FESEM) (Model SU8220, Hitachi, Japan) together with an energy dispersive X-ray analysis (EDX) for the elemental analysis of the chemical composition of the prepared nanocomposite. The FESEM operated at an accelerating voltage of 2.0 kV to achieve high-resolution imaging with a magnification of 10 K. The high-resolution surface imaging was performed using FEI Tecnai G2 20 TWIN transmission electron microscope (TEM, USA), with an acceleration voltage of 200 kV. The TEM data were then analyzed using the GATAN software (GATAN Inc., USA). To validate the reliability of the proposed method, Shimadzu QP2010 Ultra gas chromatography-mass spectrometry (GCMS) instrument outfitted with a triple quadrupole and an HP-1ms capillary RTX-5 column (30 m in length, 0.25 mm in diameter, and with a film thickness of 0.25 m) was used.

All electrochemical experiments were performed using an Autolab PGSTAT 302 N Autolab potentiostat/galvanostat (Metrohm, Netherlands) controlled with a GPES 4.9 software. Electrochemical measurements such as cyclic voltammetry (CV), electrochemical impedance spectroscopy (EIS) and square wave voltammetry (SWV) experiments were performed using a three-electrode electrochemical cell configuration. The parameters for the CV setup were determined using a start-stop potential range of −0.4 V to + 1 V, a scan rate of 50 mV/s, a sampling interval of 0.001 V, and a quiet time of 2 s. The SWV experimental conditions involve a start-stop potential range of

−0.4 V to + 0.8 V, a pulse amplitude of 10 mV, a frequency of 5 Hz, and a quiet time of 2 s. The concentration of 3-MCPDEs was determined at 0.05 μM to 255 μM using 0.01 M PBS (pH = 7.0) with scan rate of 0.05 V/s. The EIS experiments were performed at the open circuit potential (OCP) with a root mean square voltage (V_{rms}) of 10 mV, spanning a frequency range from 100 kHz to 100 mHz. The electrochemical data were acquired using the general-purpose electrochemical software (GPES) and the frequency response analyzer (FRA), both installed on a computer and connected to the potentiostat/galvanostat instrument. The value of SWV was obtained by observing the sensor response over a period of 60 s. All CV, EIS, and SWV experiments were conducted at room temperature, and three repeated determinations were performed for each set of data.

2.3. Preparation of 3-MCPD internal standard and spiked EVO oil

The 3-MCPD-d_5 working solution was utilized as an internal standard. A calibration curve was constructed by plotting the ratios of the peak areas of 3-MCPD (*m/z* 147) to the 3-MCPD-d_5 (*m/z* 150) on the y-axis against the ratios of 3-MCPD concentration to 3-MCPD-d_5 concentration on the x-axis, as described by the following formula (Eq. 1):

$$Y = aX + b \tag{1}$$

where, a and b represent the slope and intercept of the calibration curve, respectively. Accordingly, the concentration of free 3-MCPD in the test sample can be determined using the following formula (Eq. 2).

$$C = \left[\left(\frac{A_{147}}{A_{150}}\right) - b\right] \times IS \times \frac{1}{a} \quad \times \quad \frac{1}{W} \tag{2}$$

where, *C* denotes the concentration of 3-MCPD in the test sample (mg/kg). A_{147} (*m/z* 147) and A_{150} (*m/z* 150) represent the peak areas of the 3-MCPD derivative and the 3-MCPD-d_5 derivative, respectively. The variable *IS* refers to the amount of 3-MCPD-d_5 internal standard added to the test sample (μg), and *W* corresponds to the weight of the test sample in grams. Aprroximately, 300 μg/mL of a 3-MCPDE was spiked into the EVO oil as a stock solution to achieve the desired 3-MCPDEs concentrations between 0.05 μM to 255 μM. The dilution for each spiked EVO oil sample was determined using Eq. 3. These spiked samples were prepared in glass vials with a total volume of 50 mL. To ensure thorough mixing, the samples were vortexed for 1 min using a vortex mixer (Scientific Industries, Inc, USA). After mixing, the samples were kept at room temperature until further use.

$$C_1V_1 = C_2V_2 \tag{3}$$

where *C* and *V* represent concentration and volume while subscripts 1 and 2 represent the stock solution and dilution, respectively.

2.4. Synthesis of bimetallic metal-organic frameworks (Fe-Mn-MOF/NIF)

Fe-Mn-MOF was synthesized via the hydrothermal method using $FeCl_3$ and $MnCl_3$ as precursors and terephthalic acid (TPA) as the organic linker. The synthesis was carried out on a porous nickel foam (NIF) substrate at 125°C for 8 hours. The experimental procedures for the synthesis of the MOFs (Fe-MOF, Mn-MOF, and Fe-Mn-MOF) were adopted from a previously published method by Mahmoodi & Abdi, (2019), with slight modifications. The NIF foam (1.0 cm × 5.0 cm) was cleaned on both sides by rinsing with 10 mL distilled water and 0.1 M HCl. Subsequently, the NIF foam was dried in an oven at 70 ºC for 30 min. For the synthesis of the MOF composites, approximately 0.05 mmol of $FeCl_3$ and $MnCl_3$ were dissolved and mixed in 10 mL of deionized water, named as solution A. The mixing process was carried out for 30 min. Solution B was prepared in a separate beaker, by the dissolution of 0.15 mmol of TPA with 15 mL of dimethylformamide (DMF) and stirred for 30 min. The mixture solution containing 0.05 mmol of $FeCl_3$ and $MnCl_3$ (solution A) was added dropwise into the TPA solution (solution B) using a Pasteur pipette and the resulting mixture was stirred gently for another 30 min.

Subsequently, the solution was transferred into a Teflon-lined stainless steel autoclave containing a set of six pieces of pre-cleaned nickel foam (NIF). The autoclave was then placed in an oven and maintained at a temperature of 120 ºC for 6 h. After the hydrothermal treatment, the autoclave was allowed to cool to room temperature. The NIFs were washed several times with distilled water and ethanol to eliminate the impurities. After dried in an oven at 60 °C for 24 h, the prepared MOF was named as Fe-Mn-MOF/NIF. Similar techniques were applied for making the single metal MOFs with 0.05 mmol of $FeCl_3$ and $MnCl_3$ to produce the Fe-MOF and Mn-MOF, respectively. The active mass on the NIF was determined by changing the weight before and after the reaction, resulting in an active mass ranging from 1.5 to 2.0 mg/cm^{-2} for each sensor. It is crucial to emphasize that the prepared MOFs were freshly prepared as required for subsequent use.

2.5. Optimization of Fe-Mn-MOF/NIF for 3-MCPDEs detection

To evaluate the electrochemical kinetics of 3-MCPDEs sensing on the Fe-Mn-MOF/NIF-modified sensor, CV measurements were performed at varying scan rates. The CV experiments were conducted in a 0.1 M phosphate-buffered saline (PBS) solution at pH 7.0, using 120 μL of 3-MCPDEs as the analyte. The scan rates were systematically varied from 0.0025 to 0.05 V/s (0.0025, 0.005, 0.010, 0.015, 0.02, and 0.05 V/s) to assess the relationship between peak current and scan rate. The results were analyzed to determine the influence of scan rate on peak potential shifts and current response, providing insights into the charge transfer kinetics of the modified sensor. To determine the optimal pH conditions for the Fe-Mn-MOF/NIF sensor in detecting 3-MCPDEs, a pH study was conducted using CV. Electrochemical measurements were performed with varying pH values ranging from 4.0 to 8.0. The CV experiments were carried out at a fixed scan rate of 0.05 V/s to evaluate the sensor's performance under different pH conditions.

2.6. Procedure for real sample analysis

The analysis of real samples is a vital factor as it gauges the practicality of the sensor. Due to the complex sample matrix and low analyte spike levels of 3-MCPDEs, a minimal sample pre-treatment was carried out using the SWV measurements. Following the previous method by Cheng et al. (2022), the soy sauce samples purchased from a local market were spiked with three 3-MCPDEs concentrations (0.1×10^{-10}, 1×10^{-10} and 5×10^{-10} mol/L). The samples were stirred for 10 min, and followed by centrifugation speed at 10,000 rpm for 5 min. The resulting solution was extracted with 6 mL of hexane and then evaporated using nitrogen gas. The residue was dissolved in a 1:1 ethanol-water mixture, and the prepared Fe-Mn-MOF/NIF sensors were immersed in these solutions to facilitate the rebinding of 3-MCPDEs.

3. Results and discussion

3.1. Functional group determination of modified sensor

FTIR analysis was used to study the Fe-Mn-MOF/NIF sensor, to understand the interactions through the shifting and infrared bands. Certain peaks in the spectrum indicated the presence or absence of specific compounds, offering valuable insights into the interaction between 3-MCPDEs and other components. Fig. 1A-a exhibits a pair of distinct bands at 1582 cm^{-1} and 1384 cm^{-1} corresponding to the carboxylate C═O bonding and the aromatic carbon C-C vibrational mode for the Fe-MOF/NIF respectively (Xie et al., 2017). The valence vibrations is appeared at 552.5 cm^{-1} attributing to metal–oxo bond (Fe–O), while in Fig. 1A-b, a stretching vibration is observed at 586 cm^{-1} attributing to Mn-O bonds confirming the formation of bond between the carboxyl group of terephthalic acid and Fe and the

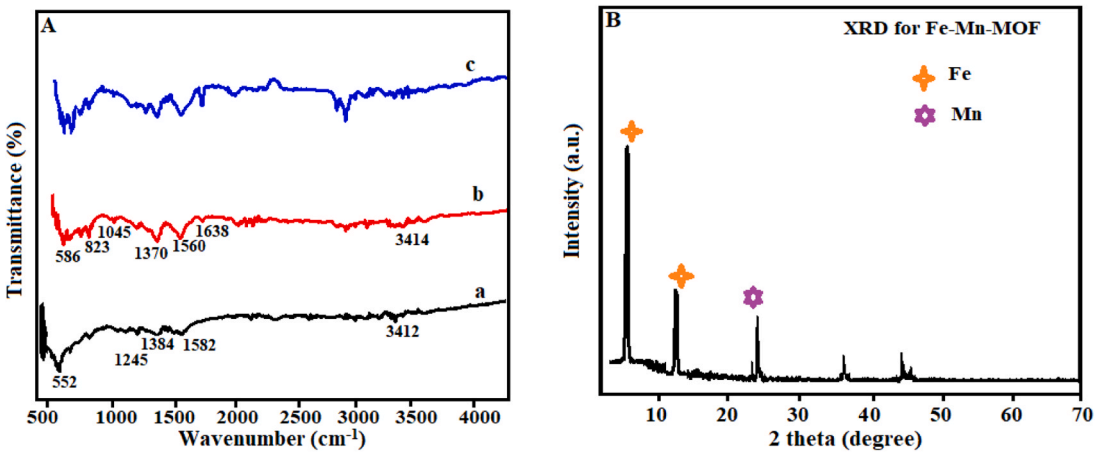

Fig. 1. FTIR spectra of (a) Fe-MOF/NIF, (b) Mn-MOF/NIF and Fe-Mn-MOF/NIF (c) (A). XRD diffractogram of Fe-Mn-MOF/NIF nanocomposite (B).

asymmetric stretching vibration of COO- peaks occurs at 1560 cm^{-1} in the Mn-MOF/NIF (Ngan Tran et al., 2022). The peaks at 1254 cm^{-1} indicate the bending vibration of the C sp^2-H bonds (Tran et al., 2023) and the O-H vibrations of Fe-MOF/NIF are associated with the broad peak centered at 3412 cm^{-1} (Jakhar et al., 2023). The Mn-MOF/NIF exhibited noticeable peaks at 1370 cm^{-1} (Fig. 1A-b) denoting the C-O stretching vibration (Yang et al., 2020). The presence of the carboxylate groups vibrations was confirmed by the bands observed at 1638 cm^{-1}, 1045 and 823 cm^{-1}, respectively. The peaks observed at 1638 cm^{-1} correspond to the carboxylate groups vibrations, while the stretching vibrations of the hydroxyl group (-OH) occur at 3414 cm^{-1} (Ai et al., 2014). Fig. 1A-c shows both of the peaks around 542 cm^{-1} and 590 cm^{-1} assuring the presence of Fe-Mn-O and successful formation of Fe-Mn-MOF.

3.2. Structure and morphology of Fe-Mn-MOF/NIF sensor

3.2.1. X-Ray diffraction analysis

The X-ray diffraction (XRD) analyses were employed to investigate the crystallinity of the Fe-MOF/NIF, Mn-MOF/NIF and Fe-Mn-MOF/NIF sensor. Fig. S1A shows characteristic peak at $2\theta = 6.5°$ and $2\theta = 15.3°$ correspond to the (111) and (222) planes of Fe, respectively indicating the coordination of Fe-MOF/NIF. While Fig. S1B represents distinguishable metallic peaks at the $2\theta = 10.8°$ and $2\theta = 20.3°$ correspond to (100), (110) and (001) crystal planes of Mn and indicating the coordination of Mn with the ligands to form Mn-MOF/NIF. Fig. 1C confirms the deposition of Fe and Mn elements onto the NIF surface. The diffraction peaks slightly shifts at $2\theta = 7°$ and 13.5°. The presence of Mn element induces a noticeable shift at $2\theta = 25°$ (040). These observations suggest that the crystal structure of NIF may have been distorted or inhibited due to the detection of 3-MCPDEs on the Fe-Mn-MOF/NIF sensor. The sharpness of these peaks indicates the successful preparation and presence of well-formed Fe-Mn-MOF/NIF. Hence, the diffraction peaks of Fe and Mn elements confirm that the structure of Fe-Mn-MOF/NIF remained intact even after the 3-MCPDEs was detected on its surface. This observation agrees with the earlier findings where, despite alterations in the lattice parameters, the fundamental framework structure of the MOF crystals remains unaltered (Haque et al., 2010; Omkaramurthy et al., 2019).

3.2.2. FESEM, EDX and TEM characterization

The morphological analysis of the Fe-Mn-MOF/NIF sensor was carried out using field emission scanning electron microscope (FESEM) shown in Fig. 2, along with energy dispersive X-ray (EDX) analysis to determine the elemental compositions of bimetallic MOF (Fe-Mn-MOF/NIF) and the individual MOFs (Fe-MOF and Mn-MOF). Fig. 2A-D illustrates the FESEM images and elemental distributions of Fe-MOF, Mn-MOF, and Fe-Mn-MOF/NIF (before and after 3-MCPDEs detection). The EDX spectrum obtained from the surface of the synthesized MOFs primarily reveals the presence of carbon (C) and NIF elements. The images reveal large sub-microrod with rectangular cross-sections of the Fe-MOF (Fig. 2A) and Mn-MOF (Fig. 2B). The FESEM/EDX results of the Fe-MOF (Fig. 2A') and Mn-MOF (Fig. 2B') show a small proportion of Fe (3.15 %) and Mn (2.25 %) element on the NIF, respectively, in the early precipitate. Fig. 2C demonstrates the combination of Fe and Mn observed on the NIF. Compared to the FESEM image (under 10 K magnification) of Fe-Mn-NIF/MOF before and after 3-MCPD detection, the morphology of Fe-Mn-MOF/NIF remains largely unchanged following the 3-MCPDEs detection (Fig. 2D). Moreover, the uniform distribution of Fe and Mn on the surface of Fe-Mn-MOF/NIF (Fig. 2C') before and after the 3-MCPDEs detection (Fig. 2D') is supported by the homogeneous distribution of the Fe and Mn elements, consistent with the FESEM images. Despite the observed negative charge, EDX analysis confirms the presence of chloride (Cl) in the Fe-Mn-MOF/NIF (Fig. 2D'). It is noteworthy that the Fe-Mn-MOF/NIF negative charge suggests that the small amount of Cl (0.78 %) is primarily balanced by the protons in the 3-MCPDEs in the spiked EVO oil. Therefore, this analysis offers valuable insights into the interfacial adhesion of Fe-Mn-MOF/NIF, which possesses a superior surface area for the detection of 3-MCPDEs compared to other single metal MOFs, confirmed by the BET analysis results in Section 3.3.

The morphological features of Fe-Mn-MOF/NIF were analysed by TEM analysis in different magnifications. Fig. 3A shows a homogeneous appearance of Fe-Mn-MOF/NIF withan average size of 3.8 nm to 4.4 nm. Fig. 3B shows the Fe-Mn-MOF on the NIF surface, with smaller aggregation dark spots and multilayer deposition of particles, indicating the presence of individual Fe and Mn compounds. The TEM images clearly show that the interaction between the 3-MCPDEs and Fe-Mn-MOF/NIF leads to the clustering of Fe and Mn particles. Fig. 3C represents a high-resolution image of Fe-Mn-MOF/NIF, where the lattice fringes are 0.226 nm and 0.242, corresponding to the (111) and (222) crystal plane for Fe. While the lattice fringes of 0.278 nm, 0.256 nm and 0.286 nm corresponding to the (100), (110) and (001) crystal plane for Mn. This matches with XRD results demonstrating the structural configuration and formation of Fe-Mn-MOF/NIF. Fig. 3D reveals the selected area electron diffraction (SEAD) with definite ring, demonstrating the crystalline nature of Fe-Mn-MOF/NIF. Although minor aggregation is observed, the Fe and Mn distribution on the NIF surface is predominantly homogeneous, ensuring sensor consistency for the detection of 3-MCPD.

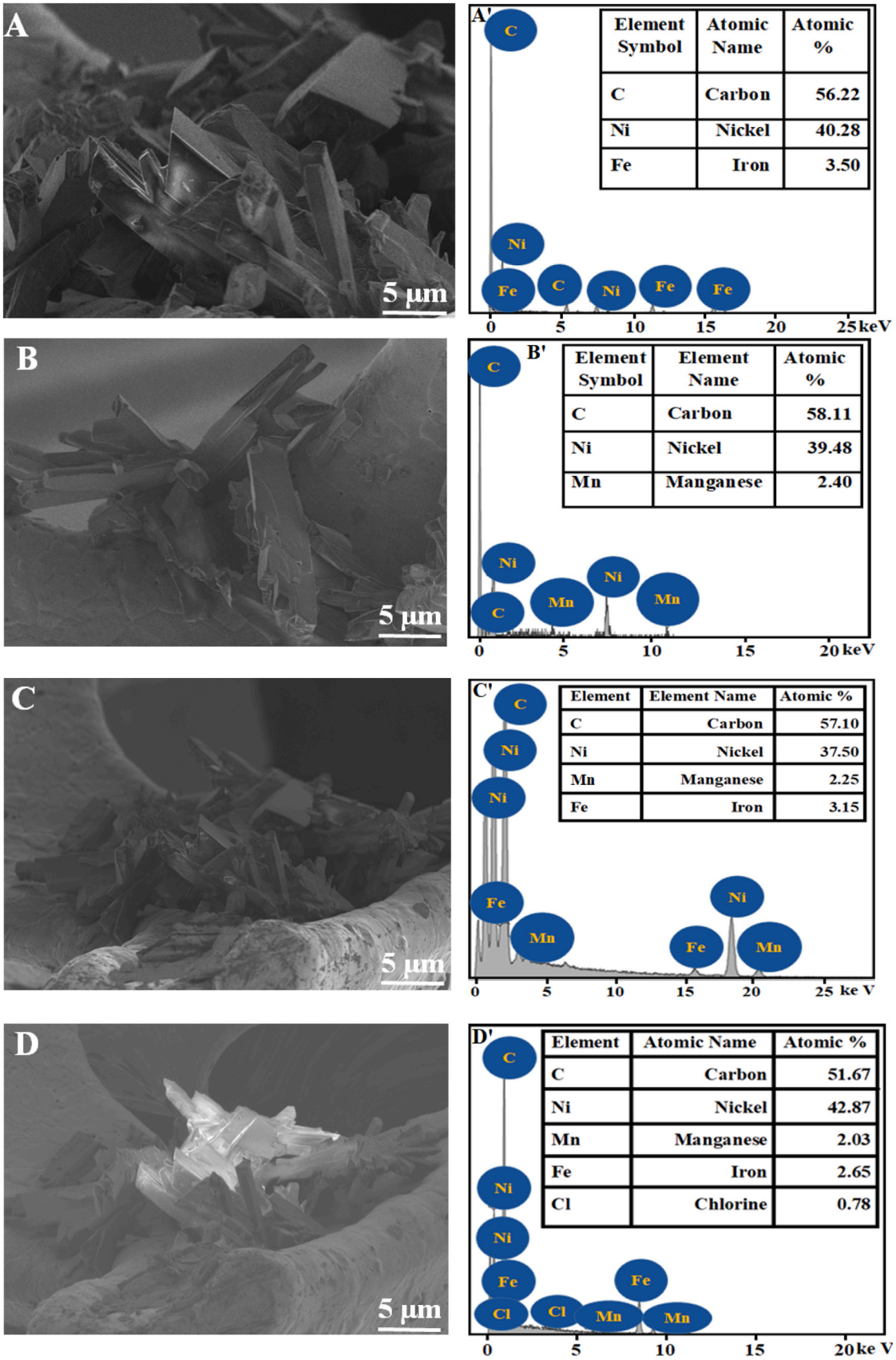

Fig. 2. FESEM image for (A) Fe-MOF/NIF, (B) Mn-MOF/NIF, (C) Fe-Mn-MOF/NIF and (D) Fe-Mn-MOF/NIF after 3MCPDEs detection. EDX for (A′) Fe-MOF/NIF, (B′) Mn-MOF/NIF, (C′) Fe-Mn-MOF/NIF and (D′) Fe-Mn-MOF/NIF after 3-MCPDEs detection.

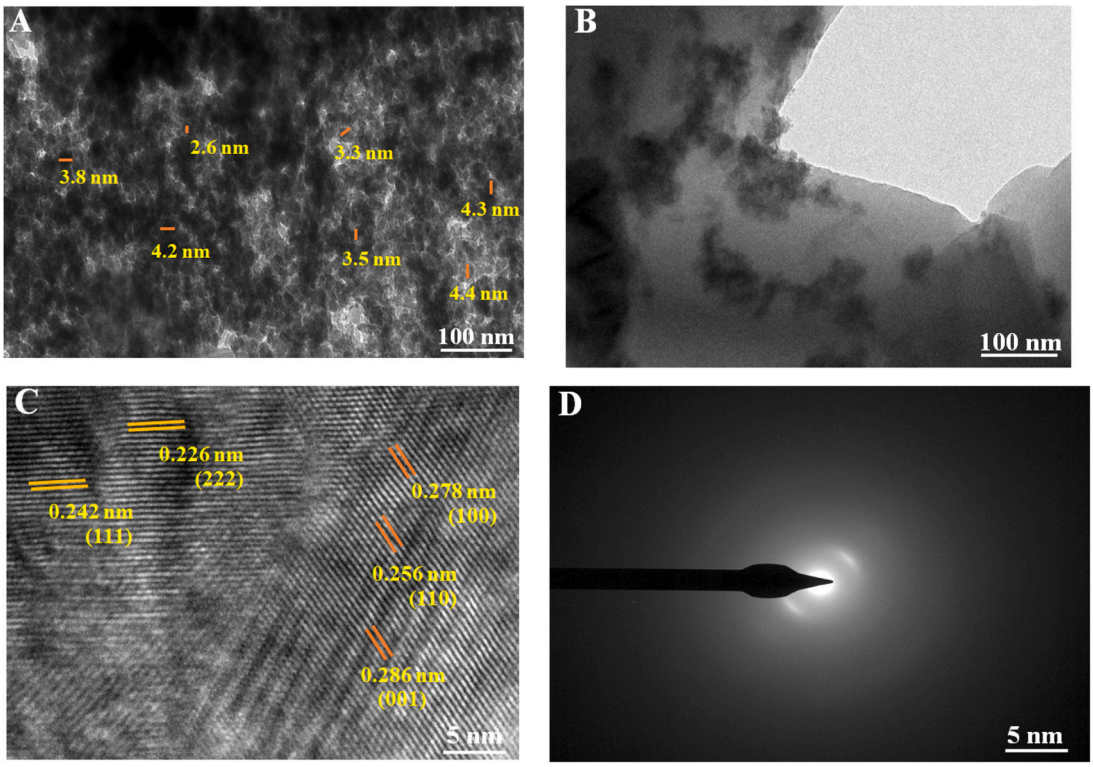

Fig. 3. TEM image for (A) Fe-Mn-MOF sensor, (B) Fe-Mn-MOF/NIF, (C) HRTEM snap displaying crystal lattices for the Fe-Mn-MOF/NIF sensor and (D) selected areas of electron diffraction (SAED) patterns of Fe-Mn-MOF/NIF sensor and enlarged images of Fig. A.

3.3. BET analysis of Fe-Mn-MOF/NIF nanocomposite

The BET adsorption-desorption isotherm study was assisted to measure the surface area, porosity, and mean pore diameter of the prepared MOFs a) Mn-MOF, b) Fe-MOF and c) Fe-Mn-MOF/NIF, as illustrated in Fig. 4(A) and Fig. (B). The N_2 adsorption-desorption isotherm of Fe-Mn-MOF shows a type IV classification according to IPUAC standards, featuring hysteresis loop type IV in the latter half (P/P_0 range of 0.5–1.0). These isotherms occur because of condensation within the small capillary pores of Fe-Mn-MOF/N4 at pressures below the N_2 gas saturation pressure. This indicates that the Fe-Mn-MOF/NIF sensor possesses a mesoporous structure (Hazra et al., 2018), which intensifies the van der Waals interaction between the molecules (Ambroz et al., 2018). Wang et al. (2019) also reported comparable findings with a mesoporous nature of a Fe-based MOF.

The calculated BET surface area values reveal that among the studied MOFs sensor, Fe-Mn-MOF/NIF (120.10 $m^2\ g^{-1}$) possesses the highest surface area compared to Fe-MOF (112.68 $m^2\ g^{-1}$) and Mn-MOF (103.70 $m^2\ g^{-1}$). This confirms the larger surface area of Fe-Mn-MOF/NIF in comparison to the single metal MOFs (Fe-MOF and Mn-MOF), suggesting that the incorporation of the Fe and Mn elements into the NIF framework facilitates the effective exposure of active sites in the resulting bimetallic Fe-Mn-MOF/NIF. Therefore, the Fe-Mn-MOF/NIF sensor exhibited the lowest Rct value compared to other electrodes, indicating enhanced electron transfer efficiency and higher electrical conductivity (Maki Ahmad et al., 2024).

The decrease in the BET surface area of Fe-MOF is attributed to the incorporation of $–NH_2$, as previously reported by Paiman et al. (2020). Additionally, the large particle sizes of the Fe and Mn elements observed in the FESEM images (Section 3.2.2) decrease the total surface area. As depicted in Table S1, the Fe-Mn-MOF/NIF demonstrates higher total pore diameter and pore volume in comparison to the individual MOFs. This suggests that the longer surface area and pore diameter enhances the adequate detection of 3-MCPEs in the spiked EVO oil when utilized in the Fe-Mn-MOF/NIF sensor. The outcomes from the N_2 isothermal adsorption-desorption is in accordance with the findings obtained from XRD and TEM analysis.

3.4. Electrochemical characterization of modified sensor

3.4.1. Electrochemical impedance spectroscopy (EIS) study of Fe-Mn-MOF/NIF sensor

The purpose of the EIS was to look into the interfacial charge transfer resistance (R_{ct}) of the modified electrode sensors. The Nyquist plot of electrodes was obtained under open circuit potential, employing an AC perturbation potential of 0.01 V at open circuit potential in 0.1 M KCl aqueous solution with 5.0 mM $[Fe(CN)_6]^{3-/4-}$ in the frequency range of 100 kHz to 100 mHz. This test provides valuable data regarding the charge-transfer resistance (R_{ct}) and the electrolyte resistance (R_s) (Banurea et al., 2023). These parameters are obtained from the Nyquist plot. Fig. 4B displays the Nyquist plots and the corresponding equivalent circuit for Mn-MOF/NIF (Fig. 4B-a), Fe-MOF/NIF (Fig. 4B-b) and Fe-Mn-MOF/NIF (Fig. 4B-c). The semi-circular diameter represents the charge transfer resistance (R_{ct}), while the straight-line at lower frequency region corresponds to the Warburg impedance attributed to a diffusion limiting phenomenon (Han et al., 2021). As seen in Fig. 4B, the R_{ct} value decreases as the NIF is sequentially deposited with Mn-MOF (curve a), Fe-MOF (curve b), and Fe-Mn-MOF/NIF (curve c). The R_{ct} values for Mn-MOF/NIF, Fe-MOF/NIF and Fe-Mn-MOF/NIF are 650 Ω, 450 Ω and 210 Ω, respectively. The decrease in the R_{ct} values is attributed to the improved electrocatalytic activity and the highest electro-conductivity of Fe-Mn-MOF/NIF compared to the Mn-MOF (curve a) and Fe-MOF (curve b). The synergy of the electro-conductivity of Fe-Mn bimetallic MOF deposited onto NIF increases the electroactive surface area significantly, which increases the electron transfer process and reduces the R_{ct} value of Fe-Mn-MOF/NIF. Fig. 4 C shows the CV experiment of Mn-MOF (curve a), Fe-MOF (curve b), and Fe-Mn-MOF/NIF (curve c) in presence of 5 mM $[Fe(CN)_6]^{3-/4-}$

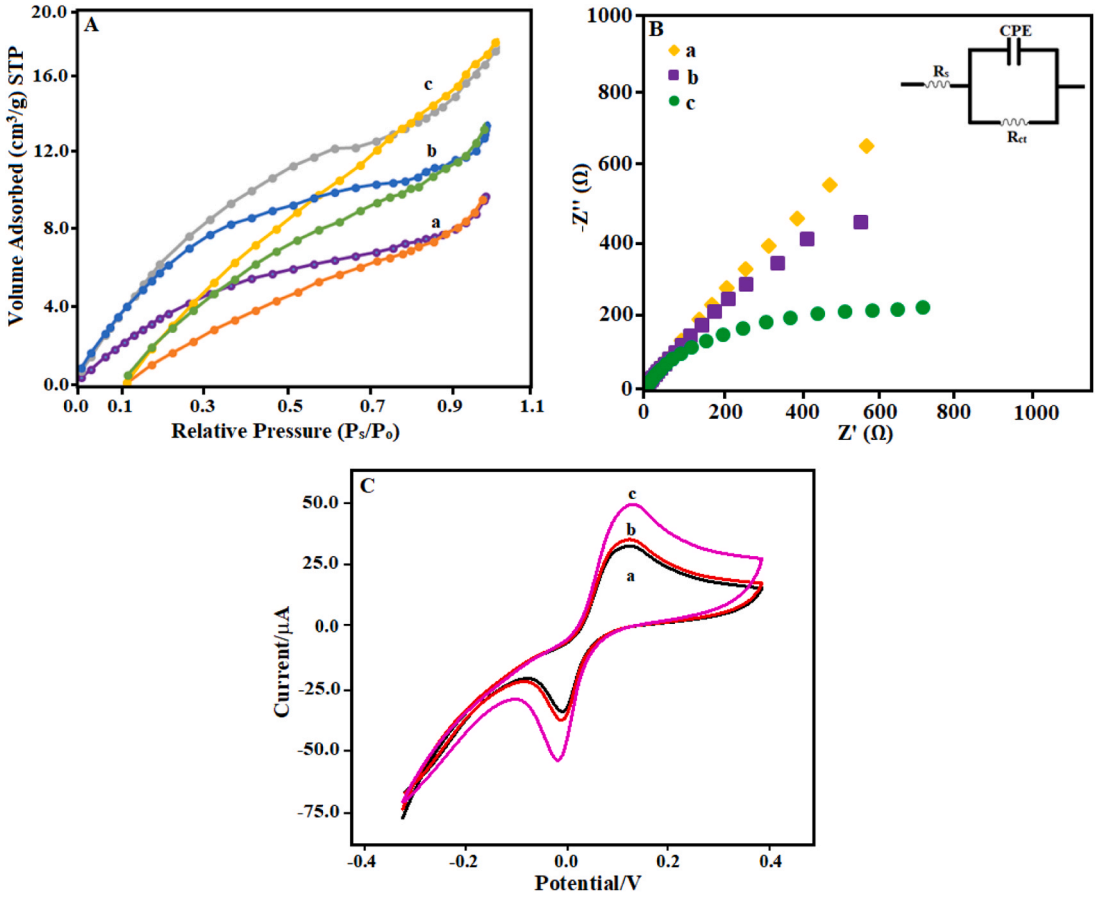

Fig. 4. (A) N_2 adsorption – desorption isotherm of (a) Mn-MOF, (b) Fe-MOF and (c) Fe-Mn-MOF/NIF at 77.31 K (-195.84 °C), and (B) EIS reactions of the several modified electrodes with 5 mM $[Fe(CN)_6]^{3-/4-}$ in 0.1 M KCl solution at (a) Mn-MOF/NIF, (b) Fe-MOF/NIF, (c) Fe-Mn-MOF/NIF (inset: Randles equivalent circuit). (C) CV curve of (a) Mn-MOF/NIF, (b) Fe-MOF/NIF, (c) Fe-Mn-MOF/NIF in 5 mM $[Fe(CN)_6]^{3-/4-}$ in 0.1 M KCl solution.

in 0.1 M KCl solution. Similar peak currents were observed for Mn-MOF and Fe-MOF (curve a and b) at 30 μA and 31 μA respectively. While the highest peak current was observed for Fe-Mn-MOF/NIF (curve c) at 53 μA compared to carve a and curve b. This result is well-matched with CV and EIS data.

3.4.2. *Cyclic voltammetry analysis of Fe-Mn-MOF/NIF sensor*

The CV was employed to investigate the electrocatalytic behavior of Fe-Mn-MOF/NIF composite towards the detection of 3-MCPDEs using various NIF-based sensors (a) NIF, (b) Mn-MOF/NIF, (c) Fe-MOF/NIF and (d) Fe-Mn-MOF/NIF. The anodic response from each sensor was measured after baseline correction. The CV was conducted with 120 μM of 3-MCPDEs (optimized at 0.001 M) in a pH 7.0 at 0.05 V/s. As seen in Fig. 5a, the NIF does not exhibit any oxidation peak in the presence of 3-MCPDEs, due to the sluggish electron transfer of on the NIF. When Mn (Fig. 5b) and Fe (Fig. 5c) elemental MOF was deposited onto the NIF substrate, a well-defined irreversible oxidation peak occurs at around 0.3 V for Mn-MOF/NIF and Fe-MOF/NIF, with an oxidation peak current of approximately 28 μA and 29 μA, for the Mn-MOF/NIF and Fe-MOF/NIF, respectively. This confirms an enhanced oxidation peak current compared to the NIF due to the electroconductivity of the Mn-MOF/NIF and Fe-MOF/NIF. A study by Teng et al. (2018) highlights the Mn and Fe interaction at the atomic level, where the combined effect produces an enhanced intrinsic electrocatalytic activity. In other words, the interaction between these two elements on an extremely small scale enhances their ability to catalyze reactions. Hence, this implies that the existence of Fe and Mn elements demonstrates faster electrocatalytic effect on the oxidation processes of 3-MCPDEs.

Additionally, the Fe-Mn-MOF/NIF exhibits the highest oxidation peak current for the 3-MCPDEs, with a slight positive shift in peak potential at 0.31 V shown in Fig. 5d. The oxidation peak current of 3-MCPDEs for Fe-Mn-MOF/NIF is 88.0 μA, marking an excellent peak current increase compared to the bare NIF and two times higher than the peak currents for the single elements of Mn-MOF/NIF and Fe-MOF/NIF sensor. This affirms the synergy between the electroconductivity of Mn-MOF/NIF and Fe-MOF/NIF, leading to an accelerated charge transfer rate, extremely porous appearance, larger effective surface area, enhanced electrocatalytic effect which offer available anchoring sites for 3-MCPDEs to oxidize and thus show improved electrochemical performance. In conclusion, among the various modified electrode sensors, the Fe-Mn-MOF/NIF sensor stands out as the most effective for the electrochemical response of 3-MCPDEs. Based on the literature and these findings, two possible pathways are proposed for the oxidation of 3-MCPD on the Fe-Mn-MOF/NIF sensor, as illustrated in Scheme 1 (SI). The first pathway is natural, which results in the formation of β-chloroactic acid, known to inhibit glycolysis, and subsequently leads to the production of oxalic acid. The second pathway involves the generation of glycidic acid or carbon dioxide through the intermediate formation of glycidol.

3.5. *Optimization of Fe-Mn-MOF/NIF for 3-MCPDEs detection*

3.5.1. *Effect of scan rate on Fe-Mn-MOF/NIF composite*

To investigate the electrochemical kinetics of 3-MCPDEs sensing on the Fe-Mn-MOF/NIF modified sensor, CV at different scan rates from 0.0025 to 0.05 V/s was performed using 120 μL 3-MCPDEs in 0.1 M PBS at pH 7.0 solution (Fig. 5 A and Fig. 5B). The outcomes clearly demonstrate that the maximum current of the 3-MCPDEs exhibits a

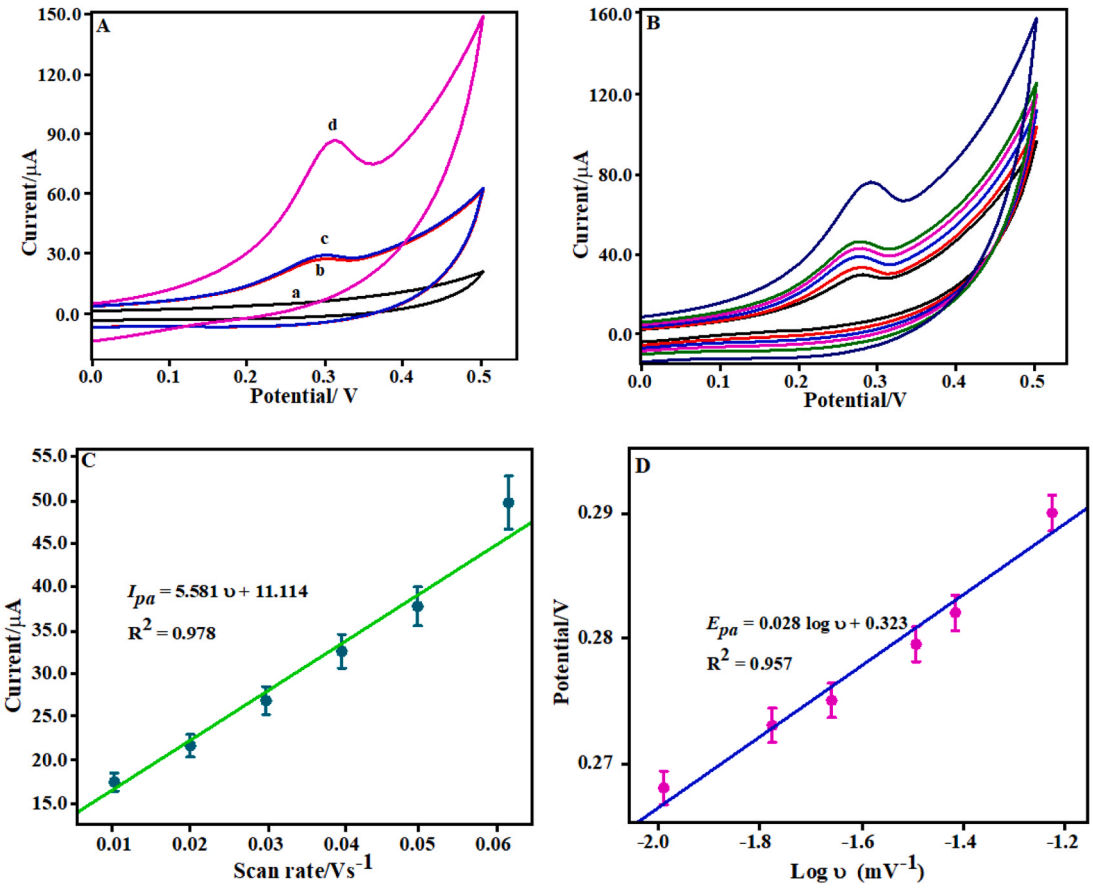

Fig. 5. (A) Cyclic voltammograms of 3-MCPDEs (120 μM) for several modified electrodes (a) NIF, (b) Mn-MOF/NIF, (c) Fe-MOF/NIF and (d) Fe-Mn-MOF/NIF at 0.1 M PBS, pH = 7.0, scan rate: 0.05 V/s. (B) Cyclic voltammograms of 3-MCPDEs (120 μM) in 0.1 M (PBS) at pH = 7.0 on Fe-Mn-MOF/NIF at different scan rates: 0.0025, 0.005, 0.010, 0.015, 0.02, 0.05 V/s. (C) The plot of the maximum currents versus scan rate. (D) The plot of the maximum potential vs Log υ.

linear increase with the scan rate from 0.0025, 0.005, 0.010, 0.015, 0.02, 0.05 V/s, with a slight shift in the peak potential at higher scan rates, where the anodic peak potentials shift from 0.27 V to 0.29 V. Fig. 5 C shows the relationship between the peak current (Ip) and the scan rate (υ), which is described by Eq. 4:

$$I_p = 5.581\ \upsilon + 11.114\ (R^2 = 0.978) \quad (4)$$

The above equation indicates that the detection of 3-MCPDEs is accomplished by a combination of surface adsorption and electron transfer processes occurring in the electrolyte solution, leading to the measured current output (Arris et al., 2022). This suggests that the 3-MCPDEs analyte easily moves from the solution to the Fe-Mn-MOF/NIF sensor surface, driven by the attractive forces between the high polarity of 3-MCPDEs (Tsai et al., 2021) and the carboxyl group (COO^-) of the TPA (Najah et al., 2022) organic linker of the MOF. The presence of the 3-MCPDE molecules on the Fe-Mn-MOF/NIF becomes dominant upon reaching the surface. Thus, the adsorption of 3-MCPDEs is the critical step that influences the overall rate of the sensor detection. The correlation coefficient value of $R^2 = 0.978$ indicates a strong correlation between the peak current and the scan rate. This suggests that the electrochemical detection of 3-MCPDEs on the sensor is primarily influenced by the surface characteristics of Fe-Mn-MOF/NIF composite.

Thus, the number of electrons participating in the oxidation reaction was determined using the Laviron's equation that was employed to calculate the electron transfer coefficient and the number of transferred electrons (Anuar et al., 2018). The straight lines in Fig. 5D represent the oxidation peak potential (E_{pa}) and their relationship to the logarithm of the scan rate (log υ) as in Eq. 5. The mathematical equation was derived from this linear curve to describe the relationship between the peak potential and the log of the scan rate.

$$E_{pa} = 0.028 \log \upsilon + 0.323\ (R^2 = 0.957) \quad (5)$$

The slopes calculated in Eq. 5 is −2.303RT/αnF. In this context, α represents the charge transfer coefficient with a specific value of 0.53, and *n* corresponds to the number of electrons in the electron transfer step. The calculated value for *n* is approximately 3.5, which can be approximated to 4, indicating that the electro-oxidation reaction of 3-MCPDEs involves 4 electrons.

3.5.2. *Influence of pH on Fe-Mn-MOF/NIF composite*

To achieve the best conditions of Fe-Mn-MOF/NIF sensor for the detection of 3-MCPDEs, pH study (pH 4.0–8.0 in 0.1 M PBS) of the electrolyte solution was carried out by using CV at 0.05 V/s, for the purpose of pH optimization. Fig. 6 A shows that the pH has a significant effect on the detection of 3-MCPDEs using the Fe-Mn-MOF/NIF sensor. Fig. 6B shows that the anodic possesses a low value in both acidic conditions (pH 4.0 to pH 6.0) and basic conditions (pH 8.0). However, there is a substantial increase in the anodic peak current at pH 7.0, which was selected as the ideal pH for all experiments.

The Fe-Mn-MOF/NIF composite exhibits positive charges on the sensor surface due to the protonation of the carboxylic group (COOH) at low pH conditions. Sakaino et al. (2022) proposed that the oxidation of triacylglycerols results in the formation of the COOH group on the glycerol backbone, which can be detected in oil samples. According to Arris et al. (2020), the 3-MCPD is a compound derived from glycerol, where one of the three hydroxyl groups (-OH) in glycerol is replaced by a Cl atom. Conversely, at upper solution pH, the COOH group in the terephthalic acid linker is deprotonated, forming the carboxylate anion

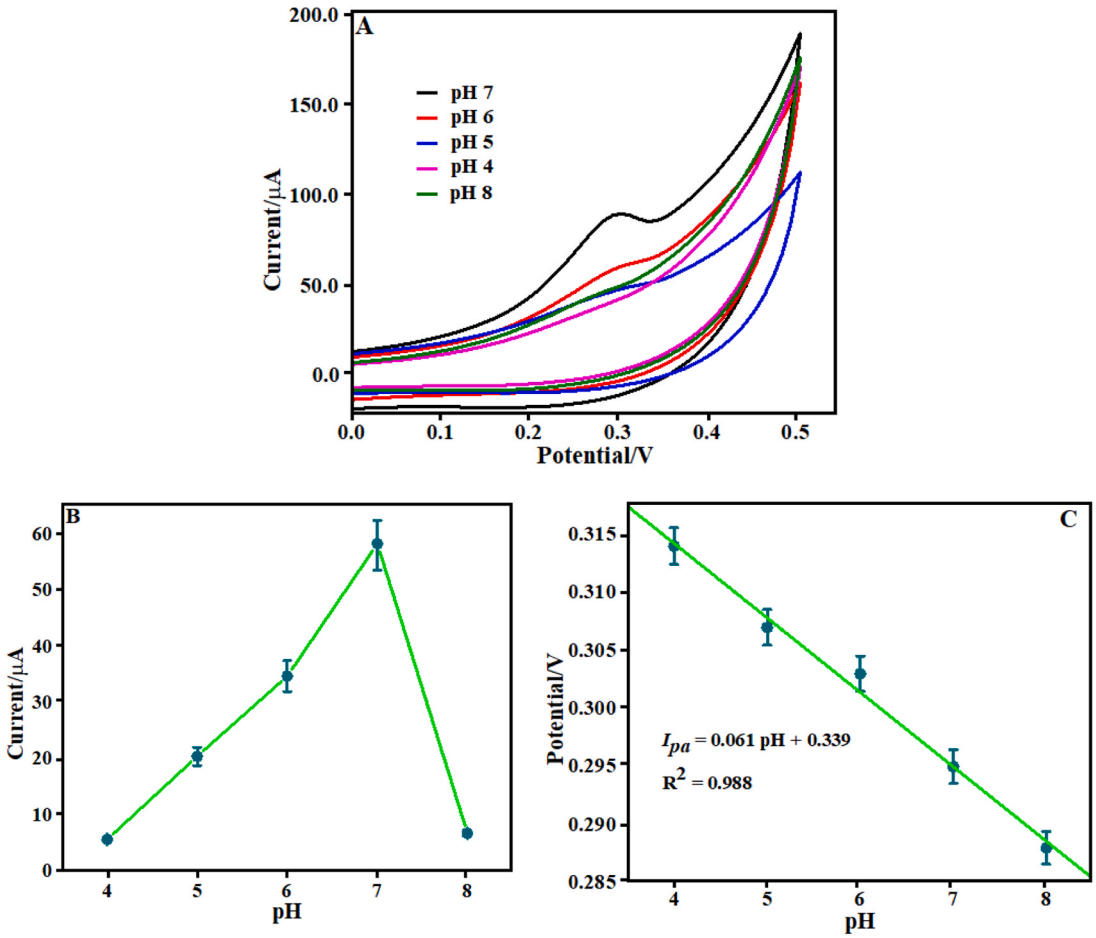

Fig. 6. (A) CV of 3MCPD (120 μM) in using Fe-Mn-MOF/NIF fabricated electrode in several pH values (4.0, 5.0, 6.0, 7.0, and 8.0, scan rate: 0.05 V/s. (B) Maximum current variation in relation to pH. (C) Formal potential versus pH value graphs.

(COO^-). Simultaneously, the OH group in 3-MCPDEs also deprotonates. It is well-known that in an alkaline environment, the Cl atom in the 3-MCPD molecule can be replaced by a carboxylic group forming 2, 3-dihydroxypropyl ester (Martin et al., 2021). Consequently, a higher pH induces an electrostatic repulsion between the Fe-Mn-MOF/NIF composite and the 3-MCPD. This leads to a decreased electro-oxidation of the analytes at the electrode surface, resulting in smaller anodic peak currents. Hence, the oxidation peak currents drop in both lower and higher solution pH.

Under neutral conditions (pH 7.0), the interaction between the weak acid and base leads to neutralization, resulting in the topmost anodic peak current as showed in Fig. 6B. This occurs as the weak acid remains unaltered, undergoing neither protonation nor deprotonation. The linear relationship between E_{pa} and pH is depicted in Fig. 9C. The respective linear regression equations for 3-MCPDEs, considering a 95 % confidence interval is expressed in Eq. 6:

$$E_{pa} = 0.061\ pH + 0.339\ (R^2 = 0.988) \quad (6)$$

The calculated slope is 0.061 V, closely aligning with the standard value of the Nernst equation (0.059 V) as reported by Douglas et al. (2017). This alignment serves as confirmation that an equal number of electrons and protons participate in the electro-oxidation reaction of 3-MCPDEs. Furthermore, this suggests that an equal number of electrons and protons are involved in the electrochemical oxidation reaction of 3-MCPDEs on the Fe-Mn-MOF/NIF nanocomposite.

3.6. Performance evaluation of the fabricated sensor

3.6.1. Analytical detection of the modified sensor

Square-wave voltammetry (SWV) was performed for the sensitive detection of 3-MCPDEs on the Fe-Mn-MOF/NIF nanocomposite. SWV is an effective electrochemical method that finds utility in various analytical and detection applications due to its rapid response and robustness (Dean et al., 2019). Additionally, incorporating parallel electrochemical techniques, like SWV, overcomes identification limitations and sensitivity associated with the Fe-Mn-MOF/NIF sensor which is capable of detecting both low and high concentrations of 3-MCPDEs. The measurements were conducted in a 0.1 M PBS solution (pH = 7), with at 0.05 V/s for different 3-MCPDEs concentration (0.05 μM to 255 μM). Fig. 7 A illustrates an oxidation peak current at 0.28 V. As depicted in Fig. 7B, a linear relationship between the peak current and concentration is observed in the range of 0.05 μM to 255 μM which proves the excellent electrocatalytic activity of the Fe-Mn-MOF/NIF sensor towards the 3-MCPDEs oxidation process. This indicates the presence of a discernible lower limit, which corresponds to the minimum concentration (0.05 μM) that can be distinguished from the background signal. The calibration ranges were characterized by a linear regression equations as follows (Eq. 7):

$$I_{pa} = 0.525\ C + 3.013\ (R^2 = 0.995) \quad (7)$$

The limit of detection (LOD) is 0.002 ± 0.001 μM, determined through the linear regression equation (Eq. 7) with a signal-to-noise ratio (S/N) of 3. Here, S represents the standard deviation of the blank response, and N corresponds to the slope of the calibration curve. The

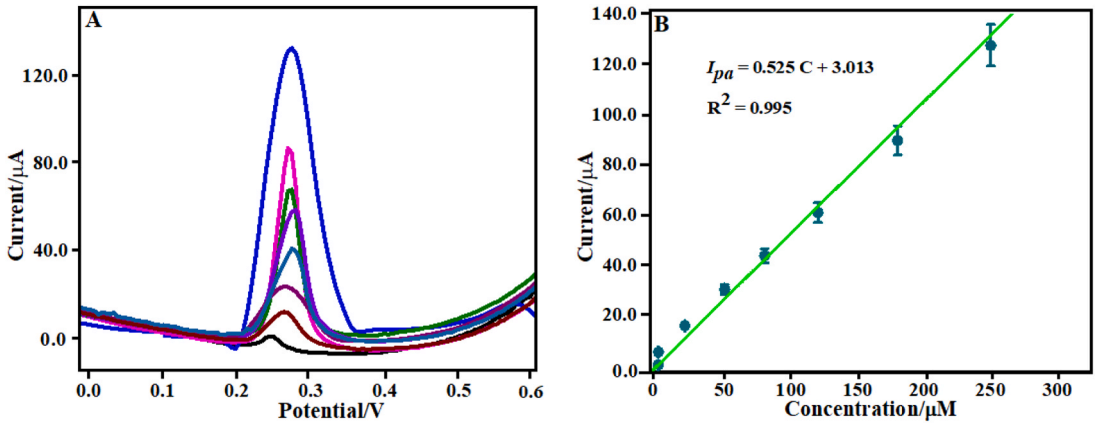

Fig. 7. (A) Square wave voltammograms, (B) Plot of peak current vs. 3-MCPDEs concentration (0.05, 0.15, 35.0, 50.0, 85.0, 135.0, 185.0 and 255 μM) using the Fe-Mn-MOF/NIF composite for detection in 0.1 M PBS (pH 7.0) with a scan rate of 0.05 V/s.

limit of quantification (LOQ) is 0.005 μM using a signal-to-noise ratio (S/N) of 10 based on linear plots in the range of 0.05 μM to 255 μM. The sensitivity was determined using Eq. 8:

$$\text{Sensitivity} = m/A \quad (8)$$

where m represents the slope of the calibration curve, and A corresponds to the surface area of the sensor (Rahman et al., 2020). The sensitivity, derived from the linear regression equation is 43.71 μA μM^{-1} cm^{-2}. The Fe-Mn-MOF/NIF sensor demonstrates the capability to enhance sensitivity and offers additional reaction sites on the surface of the modified electrode which leads to greater sensitivity. The enhnaced sensitivity stands out as a crucial parameter for sensors, signifying their capacity to detect smaller changes in the measured quantity i.e. current. This indicates that the sensor delivers more precise and accurate measurements, particularly in low concentrations or slight variations in the sample (Yang et al., 2021). To assess the Fe-Mn-MOF/NIF sensor's efficacy in the quantitative determination of 3-MCPDEs, a comparison was made with previous studies, considering parameters such as linear range and LOD.

Table 1 provides a comparison between this work and previous research regarding the LOD and linear range in the detection of 3-MCPDEs using various fabricated sensors such as molecularly imprinted electrode sensor. The summary affirms that our work has achieved the best detection performance of 3-MCPDEs compared to previous works. To the best of our knowledge, there are limited reports on the use of bimetallic MOF for 3-MCPDEs for the detection in food products. Martin et al. (2021) introduced a highly sensitive modification of a gold (Au) electrode utilizing cysteine-coated silver nanoparticles (Cys-AgNPs) for the detection of 3-MCPD in palm oil and smoked mackerel samples. The determined LOD and linear range is 0.02 μM and 0.02–1.81 μM, respectively. In a recent investigation conducted by Banurea et al. (2023), a sensor was developed using modified graphite pencil electrodes modified with a polymer of *p*-amino thiophenol and gold particles with linear range of 1.09–10.04 μM. This sensor achieved a LOD of 1.09 μM.

Yuan et al. (2019) prepared a magnetic molecularly imprinted nanoparticles (MMIPs NPs) with magnetic Fe_3O_4 (iron (II,III) oxide) and SiO_2 (silicon dioxide) with a LOD of 2.26 μM at a linear range of 9.05–1.45 × 10^5 μM. Han et al. (2021) prepared a carboxylated multi-wall carbon nanotubes (cMWCNT) incorporated in MOF with linear range of 1 × 10^{-3} to 10 μM. They reported a LOD of estimated at 4.3 × 10^{-4} μM for the detection of 3-MCPD. A sensor based on MIPs and carbon dots (MIPs/CDs) grafted onto paper was reported by Fang et al. (2019) and utilized for 3-MCPD detection. The sensor exhibited a linear range of 9.05–1.36 × 10^5 μM and achieved a LOD of 5.43 × 10^{-3} μM. Besides that, Cheng et al. (2022) reported a nanoporous gold (NPG) incorporated with MIP using DPV method which gave a LOD of 3.5 × 10^{-11} μM with linear range from 1 × 10^{-10} to 0.7 μM. All previous results confirmed that the Fe-Mn-MOF/NIF sensor in this work was reliable according to its lower LOD in the detection of 3-MCPDEs concentration in various food products.

The Fe-Mn-MOF/NIF sensor developed in this study demonstrates significant advantages over previously reported methods for the detection of 3-MCPD esters, as summarized in Table 1. One of the key highlights in this study is its wide linear detection range (0.05–255 μM) for the detection of 3-MCPD, which surpasses many existing electrochemical and fluorescence-based sensors. Notably, this is the first time this sensor has been utilized for detecting 3-MCPD. This broad range enables the detection of both trace and high concentrations of 3-MCPD esters, making it highly versatile for food safety applications. Additionally, the ultra-low detection limit (0.02 μM) is comparable to the best-performing sensors, such as Cys-AgNPs/Au, and significantly lower than other reported methods, ensuring high sensitivity for accurate contamination monitoring. Unlike conventional monometallic MOF-based sensors, Fe-Mn-MOF/NIF incorporates bimetallic Fe and Mn leading to superior electrochemical performance with enhanced sensitivity and selectivity. Another major advantage is the use of NIF as a conductive and porous substrate, which improves electron transfer,

Table 1
Comparison of 3-MCPD detection performance using the Fe-Mn-MOF/NIF sensor and other nanocomposite-based sensors, highlighting method, linear range and detection limits.

Sensor	Method	Linear Range (μM)	Detection Limit (μM)	References
Cys-AgNPs/Au	DPV	0.02 – 1.81	0.02	Martin et al. (2021)
MIP/AuNPs/GPE	EIS	1.09 – 10.04	1.09	Banurea et al. (2023)
MMIPs NPs	DPV	9.05 – 1.45 × 10^5	2.26	Yuan et al. (2019)
cMWCNT/MOF−199	DPV, EIS	1 × 10^{-3} – 10	4.3 × 10^{-4}	Han et al. (2021)
MIPs/CDs grafted paper	Fluorescence intensity	9.05 – 1.36 × 10^5	5.43 × 10^{-3}	Fang et al. (2019)
MIP/NPG/GCE	DPV	1 × 10^{-10} – 0.7	3.5 × 10^{-11}	Cheng et al. (2022)
Fe-Mn-MOF/NIF	SWV	0.05–255	0.002	This work

Abbreviations: Cys-AgNPs/Au: cysteine-coated silver nanoparticles; MMIPs NPs: magnetic molecularly imprinted nanoparticles; cMWCNT: carboxylated multi-wall carbon nanotubes; CDs: carbon dots; NPG: nanoporous gold; DPV: differential pulse voltammetry; EIS: electrochemical impedance spectroscopy; SWV: square wave voltammetry.

reduces resistance, and increases the active surface area, making the sensor more efficient than those utilizing glassy carbon electrodes or paper-based platforms. The simple and cost-effective SWV method used for detection allows rapid analysis with minimal sample preparation, reducing the time and cost compared to other methods. In brief, the Fe-Mn-MOF/NIF sensor offers a novel, highly sensitive, and efficient platform for the detection of 3-MCPD esters, outperforming existing methods in terms of sensitivity, stability, cost-effectiveness, and real-world applicability.

Besides that, performance of the Fe-Mn-MOF/NIF bimetallic sensor was evaluated against conventional detection techniques, including GC-MS and HPLC, for 3-MCPD detection. A detailed comparison of key parameters such as recovery, detection limit, and linear range is provided in Table 2. The Fe-Mn-MOF/NIF bimetallic sensor demonstrated a high recovery of approximately 94.43 %, which is comparable to conventional detection techniques such as GC-MS/MS and HPLC-MS/MS. Its broad linear range of 0.05–255 μM surpasses most GC-MS/MS methods, which generally cover narrower ranges (e.g., 0.91–45.23 μM by Zheng et al. (2020) and 0.09–0.91 μM by Ioime et al. (2021)). Additionally, the detection limit of 0.02 μM for the Fe-Mn-MOF/NIF sensor is higher to several GC-MS/MS-based approaches, including those by Le Dinh et al. (2020) (0.25 μM) and Korte et al. (2021) (3.62×10^{-3} μM). It is also comparable to the best-performing HPLC-MS/MS techniques, which achieved detection limits as low as 4.52×10^{-3} to 9.05×10^{-3} μM (Tang et al., 2023). Furthermore, the Fe-Mn-MOF/NIF sensor offers a promising alternative due to its ease of use, lower operational cost, and high sensitivity, making it a viable tool for rapid and efficient 3-MCPD detection compared to labor-intensive chromatographic techniques.

In this study, the measurement of the 3-MCPDEs concentration from 0.05 μM to 255 μM was also evaluated using GC-MS analysis. The recovery of Fe-Mn-MOF/NIF composite was tested using triplet determination in spiked samples (3-MCPDEs). Table 3 shows the recovery rates, linear range and detection limit of 3-MCPDEs in spiked EVO oil as determined using the Fe-Mn-MOF/NIF sensor, compared with those obtained through GC-MS analysis. The Fe-Mn-MOF/NIF sensor demonstrated a slightly higher recovery (92.7 %) compared to GC-MS (92.3 %), indicating that both methods are highly efficient in detecting the target analyte with minimal loss. This minor difference may be attributed to the sensor's enhanced affinity for the analyte or variations in matrix effects. In terms of the linear range, the Fe-Mn-MOF/NIF sensor exhibited a significantly broader range (0.05 – 255 μM) compared to GC-MS (0.84 – 60.6 μM), making it more versatile for detecting a wide range of analyte concentrations. Additionally, the detection limit for the Fe-Mn-MOF/NIF sensor (0.02 μM) was nearly identical to that of GC-MS (1.91×10^{-2} μM or 0.0191 μM), demonstrating comparable sensitivity between both methods. Hence, it effectively identifies the target compound (3-MCPD) without interference from other substances in the sample matrix.

Table 2
A study comparing the 3-MCPD detection to the conventional detection techniques.

Detection technique	Recovery (%)	Linear Range (μM)	Detection Limit (μM)	References
GC-MS/MS	99.9 – 87.9	0.91–0.02	0.25	Le Dinh et al. (2020)
GC-MS/MS	98–106	0.84–50.97	$< 1.81 \times 10^{-2}$ and 4.52×10^{-3}	Almoselhy et al. (2021)
GC-MS/MS	85.4–110	0.91–45.23	1.81×10^{-2}	Zheng et al. (2020)
GC-MS/MS	81 – 115	0.09–0.91	1.36×10^{-2}	Ioime et al. (2021)
GC-MS	95	0.03–3.17	3.62×10^{-3}	Korte et al. (2021)
HPLC-MS/MS	83 & 94	0.23–1.81	4.52×10^{-3} - 9.05×10^{-3}	Tang et al. (2023)
HPLC-UV	78.5–82.3	5.43–181.84	0.72	Chung et al. (2018)
Fe-Mn-MOF/NIF bimetallic sensor	~92.6	0.05–255	0.002	This work

Abbreviations: GC-MS/MS: gas chromatography tandem triple quadrupole mass spectrometry; HPLC-MS/MS: high-performance liquid chromatography−tandem mass spectrometry; HPLC-UV: high performance liquid chromatography-ultraviolet.

Noteworthy, Fe-Mn-MOF/NIF sensor offers a promising alternative to GC-MS, particularly in food safety monitoring, due to its rapid response time (sensor response over a period of 60 s) and minimal sample preparation. Its high sensitivity and selectivity make it suitable for detecting 3-MCPD in food products with real-time monitoring capabilities. Unlike GC-MS, which requires at least 18 h of operation for 3-MCPD detection due to complex instrument settings, the Fe-Mn-MOF/NIF sensor offers significant potential for on-site analysis, enhancing quality control in the food industry. This sensor enables manufacturers to detect contaminants more efficiently without relying on sophisticated instrumentation. Additionally, GC-MS analysis involves extensive sample preparation, making samples more prone to contamination and requiring the use of large volumes of solvents such as hexane and ethanol as background for 3-MCPD detection. In contrast, the bimetallic sensor minimizes chemical usage and reduces the risk of contamination, lowering instrumental cost, providing a more sustainable and efficient alternative for food safety monitoring.

In conclusion, the Fe-Mn-MOF/NIF sensor demonstrates a significantly better LOD and an extensive linear range with a remarkably high sensitivity, surpassing findings from the previous reports. This better performance is attributed to the synergistic catalytic effects of Fe and Mn elements, along with an increased electroactive surface area. These factors collectively enhance the electrochemical capabilities of the Fe-Mn-MOF/NIF sensor, enabling precise determination of 3-MCPDEs even at low concentrations.

3.6.2. Detection of 3MCPD by using FTIR

Fig. 8 curve a and b shows the FTIR spectra before and after the absorption of 3MCPD on the Fe-Mn-MOF/NIF sensor. Several distinct bands were appeared such as 800 cm^{-1} assinging to C-Cl bond which is hypothetically considered as a functional band of 3-MCPD, a distinct peak appeared at 1150 cm^{-1} assigning to CH_2 wagging. In addition, curve b shows a sharp peak at 1375 cm^{-1} corresponding to CH_3 bending and C-H stretching bond at 1740 cm^{-1} becomes sharper due to the absorption of 3-MCPD containing C-H bond compared to curve a. Furthermore, the height of peaks at 2850 cm^{-1} and 2927 cm^{-1} increased remarkably due to the C═O stretching of esters, C-H asymmetric stretching of CH_2 and C-H symmetric stretching of CH_2 due to absorption of 3-MCPD compared to curve a. The obtained result is in the well-matched with the previous result (Coates, 2000).

3.6.3. Analysis of the coexisting substances' interference in spiked EVO oil

Selectivity is a crucial parameter for the success of a fabricated sensor and can be assessed through an interference study. The interference study was conducted on the Fe-Mn-MOF/NIF sensor to validate the selectivity of the suggested technique in spiked EVO oil with 3-MCPDEs in the presence of fatty acid compounds. The interference study of 3-MCPDEs was conducted in 0.1 M PBS (pH 7.0) at 0.5 V/s, as shown in Fig. 9. The inset of Fig. 9 shows SWV curve for 30 μM of 3-MCPDEs. It is showed that Fe-Mn-MOF/NIF sensor can detect 3-MCPDEs efficiently even in the presence of 5-fold concentrations of 2-MCPD, 1,2-propanediol, L-phenylalanine, L-glutamic acid, L-tryptophane and Vitamin-A. The elevated concentrations of the interfering compounds could not deviate from the current response of the Fe-Mn-MOF/NIF sensor toward the detection of 3-MCPD. Fig. 9 (bar chart) shows the SWV current response of 3MCPD and the negligible response of the

Table 3
Comparison between 3-MCPDEs detection in spiked EVO oil using GC-MS and electrochemical analysis for Fe-Mn-MOF/NIF sensor.

	Recovery (%)	Linear Range (μM)	Detection Limit (μM)	Standard deviation (%)[a]	LOD (mg/kg)[b]	LOQ (mg/kg)[b]
Fe-Mn-MOF/NIF sensor	92.7	0.05–255	0.02	1.67	0.0025	0.0048
GC-MS	92.3	0.84 – 60.6	1.91×10^{-2}	2.37	1.46	4.44

[a] Relative standard deviation of overall determinations (inter-day variation).
[b] The LOD and LOQ were estimated from the standard deviation(s) of nine measurements.

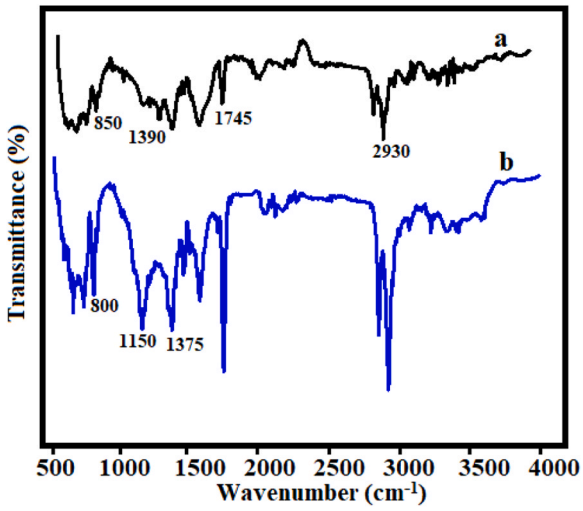

Fig. 8. FTIR spectra, (a) before and (b) after 3-MCPDEs detection at wavenumber from 500 cm^{-1} to 4000 cm^{-1}.

interfering compounds. This demonstrates that the Fe-Mn-MOF/NIF sensor has high selectivity towards 3-MCPD detection.

3.6.4. *Reproducibility and repeatability of Fe-Mn-MOF/NIF sensor*

The reproducibility and repeatability of Fe-Mn-MOF/NIF sensor was investigated using SWV technique. In this method, five Fe-Mn-MOF/NIF electrodes were prepared under identical parameters for the detection of 3-MCPDEs illustrated in Fig. 9B. The calculated relative standard deviation (RSD) values, derived from the current response of five electrodes, were 3.75 % for 3-MCPDEs. The bar diagram indicates that the current response for each electrode possesses good similarity and acceptable reproducibility. Repeatability is an important parameter of an electrode refers to its ability to produce consistent and reproducible measurements when the same procedure is conducted multiple times under identical conditions. The bar diagram in Fig. 9C shows that, current response of the modified electrode was measured once for consecutive 6 weeks to investigate the current deviation of the fabricated electrode. The prepared electrode was strictly stored in moisture-free conditions. It was observed that, even after six weeks, the peak current was deviated less than 90 % concluding that the fabricated electrode possesses long term stability with acceptable reproducibility and repeatability towards the determination of 3-MCPDEs.

3.6.5. *Cyclic stability of sensor*

The CV technique was utilized to investigate the cyclic stability of the Fe-Mn-MOF/NIF sensor. Fig. S2A illustrates that the CV of Fe-Mn-MOF/NIF is consistent after 10 cycles. These findings confirm that the sensor exhibits exceptional cyclic stability. The Fe-Mn-MOF/NIF sensor was kept at room temperature for 21 days to assess the long-term stability and the current response was analysed weekly. After the first week, the sensor maintained 95.5 % of its initial current response, followed by 90 % and 86.5 % retention after the second and third weeks, respectively (Fig. S2B, SI) and included the real data in Fig. S2C in SI, this data is very close to our previous data, which is prove that the sensor has excellent accuracy and precision. The good stability under room temperature indicates that the incorporation of Fe and Mn into the MOF protects the Fe-Mn-MOF/NIF sensor from oxidation with increasing storage time. A noteworthy finding is that the Fe-Mn-MOF/NIF sensor's acceptable long-term storage stability is confirmed by its greater relative standard deviation (RSD) value of 5 %.

3.7. *Study of real sample*

The next phase involves the evaluation of the sensor application in real samples. Soy sauce was chosen as the real sample in this study due to its high consumption and reported higher 3-MCPD levels compared to other food products. In a survey of 5712 food samples consumed in Korea, 3-MCPD was detected in 5.3 % of the total samples, with soy sauce showing the highest detection rate at 25 % (Jang and Koh, 2020). In this study, three different concentrations of 3-MCPDEs were spiked into soy sauce samples, and impedance measurements were conducted in triplicate (n = 3). This analysis involves the standard addition of the 3-MCPDEs in the presence of 0.1 M PBS (pH 7.0) at a scan rate of 0.05 V/s using the SWV method. The voltametric response of the Fe-Mn-MOF/NIF sensor was completed using different 3-MCPDEs concentration, and the percentage recovery and RSD values was subsequently calculated (Table S2).

The percentage recovery values were determined by comparing the relative SWV peak currents before and after spiking of the 3-MCPDEs into the soy sauce. The recovery values for three soy sauce samples ranged from 92.6 % to 96.2 %, with an average recovery of 94.43 % and low RSD% values, demonstrating the reliability of the Fe-Mn-MOF/NIF sensor. These results demonstrate its practical application in real food matrices. Moreover, the European Community has set a maximum limit of 5.64 μM of 3-MCPDEs in soy sauce (Joint Fao/Who Expert Committee On Food, 2016). Consequently, the Fe-Mn-MOF/NIF sensor, with its lower LOD of 0.02 μM provides a significant advantage in real sample applications.

4. Conclusion

This study successfully developed a Fe-Mn-MOF/NIF nanocomposite-based electrochemical sensor for the efficient detection of 3-MCPDEs in real food samples. The integration of bimetallic MOFs with NIF provided a robust sensing platform with enhanced electrocatalytic activity, enabling precise and rapid detection. The sensor ease of fabrication, cost-effectiveness, and suitability for on-site applications make it a viable alternative to conventional analytical methods. The fabricated Fe-Mn-MOF/NIF showed high catalytic activity for the oxidation of 3-MCPDEs. Hence, the oxidation peaks current of 3-MCPDEs significantly increased due to the higher electrocatalytic activity of the Fe-Mn-MOF/NIF nanocomposite. This demonstrated a lower LOD, wider linear range and better sensitivity which is comparable to more established indirect methods for the detection of 3-MCPDEs. Furthermore, the bimetallic MOF sensor also demonstrated good recoveries compared to the GC-MS analysis. The modified electrode sensor also showed outstanding cyclic stability even after 10 continuous cycles. Real samples utilizing soy sauce gave satisfactory recovery and RSD values, highlighting the significant potential of MOF-based electrochemical

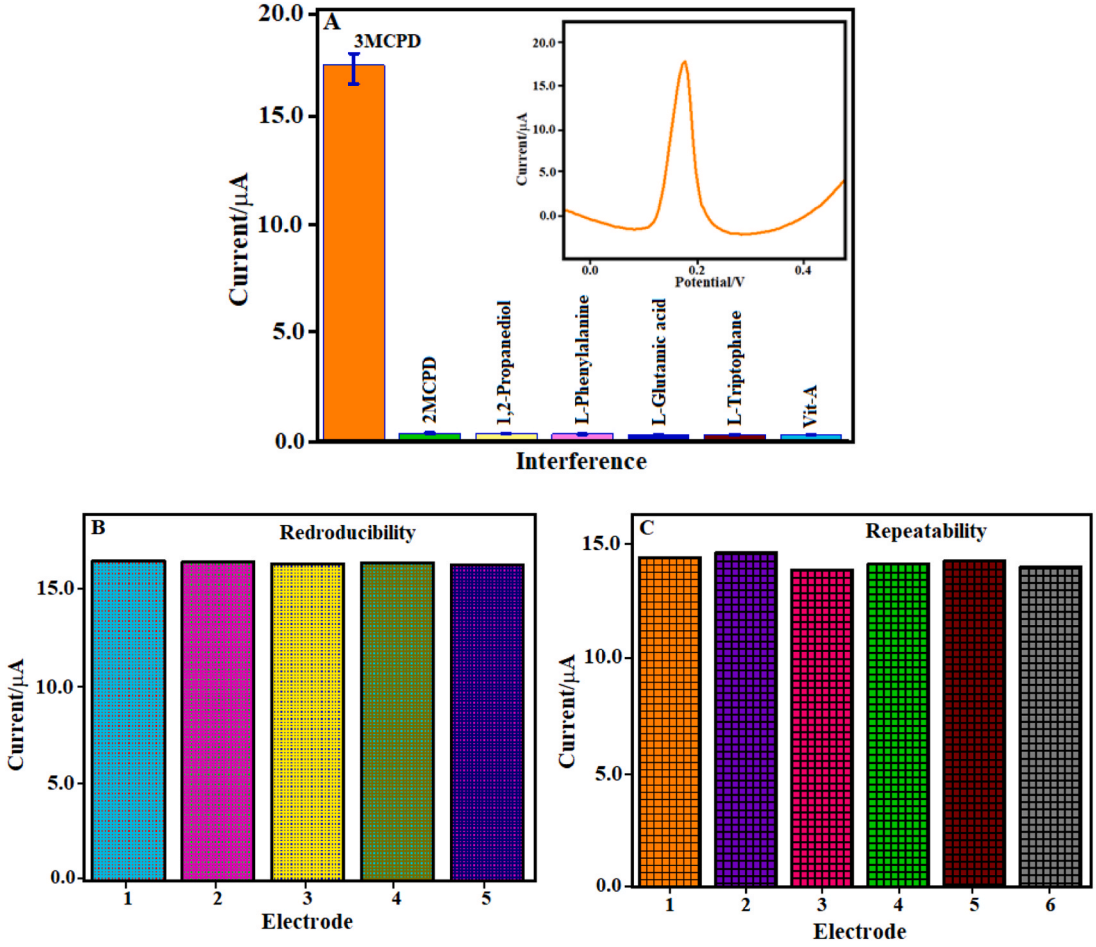

Fig. 9. Interference study with different interfering species at Fe-Mn-MOF/NIF, inset: SWV response for the detection of 3-MCPDEs.

sensors in food safety monitoring and demonstrate their capability to address current challenges in detecting food contaminants. This work lays the foundation for future advancements in sensor technology, offering a promising approach for ensuring food quality and consumer safety.

CRediT authorship contribution statement

Srinivasan Seshasai: Writing – review & editing, Supervision, Investigation. **Rajabzadeh Amin Reza:** Writing – review & editing, Supervision, Investigation. **Hayyan Adeeb:** Writing – review & editing, Resources, Formal analysis. **Alanazi Yousef Mohammed:** Writing – review & editing, Supervision, Investigation. **Chakrabarti Barun Kumar:** Writing – review & editing, Supervision. **Low Chee Tong John:** Writing – review & editing, Supervision. **Putra Sharifah Shahira Syed:** Writing – original draft, Methodology, Investigation, Formal analysis, Conceptualization. **Shalauddin Md.:** Writing – review & editing, Writing – original draft, Supervision, Investigation, Formal analysis. **Akhter Shamima:** Writing – review & editing, Writing – original draft, Supervision, Investigation, Data curation. **Basirun Wan Jefrey:** Writing – review & editing, Supervision, Investigation, Funding acquisition. **Elgharbawy Amal A. M.:** Writing – original draft, Validation, Investigation. **Ahmed Syed Rahin:** Writing – review & editing, Supervision.

Declaration of Competing Interest

The authors declare that they have no known competing financial interests or personal relationships that could have appeared to influence the work reported in this paper.

Acknowledgements

The authors would like to thank the International Institute for Halal Research and Training (INHART), Nanotechnology and Catalysis Research Center (NanoCat) and Researcher's Supporting Project Number (RSP2025R511), King Saud University, Riyadh, Saudi Arabia, for their contributions to this work. This work was financially supported by the Ministry of Higher Education, Malaysia, for niche area research under the Higher Institution Centre of Excellence (HICoE) program (JPT (BKPI)1000/016/018/28 Jld.3(2) & NANOCAT-2024B)

Appendix A. Supporting information

Supplementary data associated with this article can be found in the online version at doi:10.1016/j.jfca.2025.107702.

Data availability

Data will be made available on request.

References

Ahn, Y., Choi, S., Kwak, S.Y., 2020. Remarkable effect of deprotonation on adsorption of 3-MCPD and glycidol on carboxylated Fe-MIL-88s. J. Environ. Chem. Eng. 8, 104456. https://doi.org/10.1016/j.jece.2020.104456.

Ai, L., Zhang, C., Li, L., Jiang, J., 2014. Iron terephthalate metal-organic framework: Revealing the effective activation of hydrogen peroxide for the degradation of organic dye under visible light irradiation. Appl. Catal. B Environ. 148–149, 191–200. https://doi.org/10.1016/j.apcatb.2013.10.056.

Almoselhy, R.I.M., Eid, M.M., Abd El-Baset, W.S., Aboelhassan, A.E.F.A., 2021. Determination of 3-MCPD in some edible oils using GC-MS/MS. Egypt. J. Chem. 64, 1639–1652. https://doi.org/10.21608/EJCHEM.2021.64084.3373.

Ambroz, F., Macdonald, T.J., Martis, V., Parkin, I.P., 2018. Evaluation of the BET theory for the characterization of meso and microporous MOFs. Small Methods 2, 1–17. https://doi.org/10.1002/smtd.201800173.

Amini, A., Kazemi, S., Safarifard, V., 2020. Metal-organic framework-based nanocomposites for sensing applications – A review. Polyhedron 177, 114260. https://doi.org/10.1016/j.poly.2019.114260.

Anuar, N.S., Basirun, W.J., Ladan, M., Shalauddin, M., Mehmood, M.S., 2018. Fabrication of platinum nitrogen-doped graphene nanocomposite modified electrode for the electrochemical detection of acetaminophen. Sens. Actuators, B Chem. 266, 375–383. https://doi.org/10.1016/j.snb.2018.03.138.

Araujo, M., Beekman, J.K., Mapa, M.S.T., Macmahon, S., Zhao, Y., Flynn, T.J., Flannery, B., Mossoba, M.E., Sprando, R.L., 2020. Toxicology in Vitro Assessment of intestinal absorption / metabolism of 3-chloro-1, 2-propanediol (3-MCPD) and three 3-MCPD monoesters by Caco-2 cells. Toxicol Vitr. 67, 104887. https://doi.org/10.1016/j.tiv.2020.104887.

Arris, F.A., Manan, W.N., Kaco, H., Shaffie, A.H., Sajab, M.S., 2021. Electrochemical characterization of graphite-zero-valent iron for 3-Monochloropropane-1,2-Diol (3-MCPD) detection. Mater. Sci. Forum 1025, 20–25. https://doi.org/10.4028/www.scientific.net/MSF.1025.20.

Arris, F.A., Mohan, D., Sajab, M.S., 2022. Facile synthesis of 3D printed tailored electrode for 3-Monochloropropane-1, 2-Diol (3-MCPD) sensing. Micromachines 13, 383. https://doi.org/10.3390/mi13030383.

Arris, F.A., Thai, V.T.S., Manan, W.N., Sajab, M.S., 2020. A revisit to the formation and mitigation of 3-chloropropane-1,2-diol in palm oil production. Foods 9, 1–24. https://doi.org/10.3390/foods9121769.

Banurea, I.R., Sanjaya, A.R., Nizardo, N.M., Ivandini, T.A., 2023. Molecularly imprinted polymer of *p*-amino thiophenol thiophenol for a 3-monochloropropane-1,2-diol impedance-based sensor. Mater. Chem. Phys. 301, 127613. https://doi.org/10.1016/j.matchemphys.2023.127613.

Cheng, W., Zhang, Q., Wu, D., Yang, Y., Zhang, Y., Tang, X., 2022. A facile electrochemical method for rapid determination of 3-chloropropane-1,2-diol in soy sauce based on nanoporous gold capped with molecularly imprinted polymer. Food Control 134. https://doi.org/10.1016/j.foodcont.2021.108750.

Chung, H.-Y., Kumar Ponnusamy, V., Jen, J.-F., 2018. Determination of 3-chloropropanediol in soy sauce samples by liquid phase extraction coupled with microwave-assisted derivatization and high performance liquid chromatography-ultraviolet detection. Int. J. Eng. Res. Sci. 4, 54–61. https://doi.org/10.5281/zenodo.1238763.

Coates, J., 2000. Interpretation of Infrared Spectra, A Practical Approach. Encycl. Anal. Chem.

Dean, S.N., Shriver-lake, L.C., Stenger, D.A., Erickson, S., Golden, J.P., Trammell, S.A., 2019. Machine learning techniques for chemical identification using cyclic square wave voltammetry. Sensors 19, 2392. https://doi.org/10.3390/s19102392.

Douglas, A., Skoog, F.James, Holler, S.R.C., 2017. Principles of instrumental analysis, 7th ed. Cengage Learning.

Dua, Y., Hu, J., Hu, Z., Zhang, W., Qi, Y., Zhang, Y., Li, X., Liu, Yi, 2021. A sensitive HPLC-FLD method for the quantitative determination of 3-chloro-1, 2-propanediol by pre-column fluorescence derivatization with 9- (2-Hydroxypropyl) adenine. J. Liq. Chromatogr. Relat. Technol. 44, 445–456.

Fang, M., Zhou, L., Zhang, H., Liu, L., Gong, Z.Y., 2019. A molecularly imprinted polymers/carbon dots-grafted paper sensor for 3-monochloropropane-1,2-diol determination. Food Chem. 274, 156–161. https://doi.org/10.1016/j.foodchem.2018.08.133.

Genualdi, S., Nyman, P., DeJager, L., 2017. Simultaneous analysis of 3-MCPD and 1,3-DCP in Asian style sauces using QuEChERS extraction and gas chromatography-triple quadrupole mass spectrometry. J. Agric. Food Chem. 65, 981–985. https://doi.org/10.1021/acs.jafc.6b05051.

Han, S., Ding, Y., Teng, F., Yaoa, A., Lenga, Q., 2021. Determination of chloropropanol with an imprinted electrochemical sensor based on multi-walled carbon nanotubes / metal – organic framework. RSC Adv. 11, 18468–18475. https://doi.org/10.1039/d1ra02731j.

Haque, E., Khan, N.A., Park, J.H., Jhung, S.H., 2010. Synthesis of a metal–organic framework material, iron terephthalate, by ultrasound, microwave, and conventional electric heating: a kinetic study. Chem. (Easton) 18 (16), 1046–1052. https://doi.org/10.1002/chem.200902382.

Hazra, B., Wood, D.A., Vishal, V., Varma, A.K., Sakha, D., Singh, A.K., 2018. Porosity controls and fractal disposition of organic-rich Permian shales using low-pressure adsorption techniques. Fuel 220, 837–848. https://doi.org/10.1016/j.fuel.2018.02.023.

He, B., Wang, L., Li, M., 2020. A biosensor for direct bioelectrocatalysis detection of 3-MCPD in soy sauce using Cyt-c incorporated in Au@AgNSs/FeMOF nanocomposite. J. Iran. Chem. Soc. 18, 151–158. https://doi.org/10.1007/s13738-020-02011-z.

Ioime, P., Piva, E., Pozzebon, M., Pascali, J.P., 2021. Automated sample preparation and analysis by gas chromatography tandem mass spectrometry (GC–MS/MS) for the determination of 3- and 2-monochloropropanediol (MCPD) esters and glycidol esters in edible oils. J. Chromatogr. A 1650. https://doi.org/10.1016/j.chroma.2021.462253.

Jakhar, S., Singh, N., Siwal, S.S., 2023. In-situ synthesis of reduced graphene oxide templated MIL-53(Fe) nanorods for photo-catalytic degradation of organic dyes under sunlight. Vietnam J. Chem. 61, 646–654. https://doi.org/10.1002/vjch.202300126.

Jang, Y., Koh, E., 2020. Assessment of estimated daily intake of 3-monochloropropane-1,2-diol from soy sauce in Korea. Food Sci. Biotechnol. https://doi.org/10.1007/s10068-020-00832-5.

JECFA, 2017. Evaluation of certain contaminants in food: eighty-third report of the Joint FAO/WHO Expert Committee on Food Additives, WHO Technical Report Series. Joint FAO/WHO Expert Committee On Food, 2016. Evaluations of contaminants.

Korte, R., Schulz, S., Brauer, B., 2021. Chloropropanols (3-MCPD, 1,3-DCP) from food contact materials: GC-MS method improvement, market survey and investigations on the effect of hot water extraction. Food Addit. Contam. - Part A Chem. Anal. Control. Expo. Risk Assess. 38, 904–913. https://doi.org/10.1080/19440049.2021.1903569.

Le Dinh, C., Nguyen Nhu, T., Vu Ngoc, T., Le Thi, H.H., Tran Cao, S., 2020. GC-MS/MS method for simultaneous determination of ester forms of 3-MCPD and 2-MCPD in infant formula. Heavy Met. Arsen. Conc. Water, Agric. Soil, rice Ngan Son. Dist. Bac. Kan. Prov. Vietnam 3, 133–144. https://doi.org/10.47866/2615-9252/vjfc.103.

Liu, P.W., Li, C.I., Huang, K.C., Liu, C.S., Chen, H.L., Lee, C.C., Chiou, Y.Y., Chen, R.J., 2021. 3-MCPD and glycidol coexposure induces systemic toxicity and synergistic nephrotoxicity via NLRP3 inflammasome activation, necroptosis, and autophagic cell death. J. Hazard. Mater. 405, 124241. https://doi.org/10.1016/j.jhazmat.2020.124241.

Mahmoodi, N.M., Abdi, J., 2019. Nanoporous metal-organic framework (MOF-199): Synthesis, characterization and photocatalytic degradation of Basic Blue 41. Microchem. J. 144, 436–442. https://doi.org/10.1016/j.microc.2018.09.033.

Maki Ahmad, M., Roushani, M., Farokhi, S., 2024. Ni-P nanosheets derived from a metal–organic framework containing triptycene ligand: A high-performance electrochemical sensor for glucose determination. Microchem. J. 197, 1–8. https://doi.org/10.1016/j.microc.2023.109737.

Martin, A.A., Fodjo, E.K., Marc, G.B.I., Albert, T., Kong, C., 2021. Simple and rapid detection of free 3-monochloropropane-1,2-diol based on cysteine modified silver nanoparticles. Food Chem. 338, 127787. https://doi.org/10.1016/j.foodchem.2020.127787.

Najah, A., Boivin, D., Noël, C., De Poucques, L., Henrion, G., Cuynet, S., 2022. Amino-grafting pre-functionalization of terephthalic acid by impulse dielectric-barrier discharge (DBD) plasma for amino-based Metal-Organic Frameworks (MOFs). Mater. Chem. Phys. 290. https://doi.org/10.1016/j.matchemphys.2022.126629.

Ngan Tran, T.K., Ho, H.L., Nguyen, H.V., Tran, B.T., Nguyen, T.T., Thi Bui, P.Q., Bach, L. G., 2022. Photocatalytic degradation of Rhodamine B in aqueous phase by bimetallic metal-organic framework M/Fe-MOF (M = Co, Cu, and Mg). Open Chem. 20, 52–60. https://doi.org/10.1515/chem-2021-0110.

Omkaramurthy, B.M., Krishnamurthy, G., Foro, S., 2019. Electrocatalytic activity and chemical sensor application of Mn-MOF: Synthesis, crystal structure and photo luminescent properties. Mater. Res. Express 6. https://doi.org/10.1088/2053-1591/ab61ad.

Paiman, S.H., Rahman, M.A., Uchikoshi, T., Abdullah, N., Othman, M.H.D., Jaafar, J., Abas, K.H., Ismail, A.F., 2020. Functionalization effect of Fe-type MOF for methylene blue adsorption. J. Saudi Chem. Soc. 24, 896–905. https://doi.org/10.1016/j.jscs.2020.09.006.

Putra, S.S.S., Basirun, W.J., Elgharbawy, A.A.M., Hayyan, M., Alabdulmonem, W., Aljohani, A.S.M., Hayyan, A., 2023. 3-Monochloropropane-1,2-diol (3-MCPD): a review on properties, occurrence, mechanism of formation, toxicity, analytical approach and mitigation strategy. J. Food Meas. Charact. https://doi.org/10.1007/s11694-023-01883-y.

Putra, S.S.S., Basirun, W.J., Hayyan, A., Elgharbawy, A.A.M., 2022. Role of Green Nanomaterials For 3-chloropropane-1,2-diol Ester (3-MCPDE) Reduction. In: Shanker, U., Hussain, C.M., Rani, M. (Eds.), Handbook of green and sustainable nanotechnology. Springer, Cham, pp. 1–20. https://doi.org/10.1007/978-3-030-69023-6_70-1.

Rahman, M.M., Alam, M.M., Alamry, K.A., 2020. A reliable alternative approach for the ultra-sensitive detection ofl-glutathione with wet chemically synthesized Co3O4-doped SnO2nanoparticles decorated on a glassy carbon electrode. N. J. Chem. 44, 16020–16030. https://doi.org/10.1039/d0nj03726e.

Sakaino, M., Sano, T., Kato, S., Shimizu, N., Ito, J., Rahmania, H., Imagi, J., Nakagawa, K., 2022. Carboxylic acids derived from triacylglycerols that contribute to the increase in acid value during the thermal oxidation of oils. Sci. Rep. 12, 1–9. https://doi.org/10.1038/s41598-022-15627-3.

Schultrich, K., Henderson, C.J., Braeuning, A., Buhrke, T., 2020. Correlation between 3-MCPD-induced organ toxicity and oxidative stress response in male mice. Food Chem. Toxicol., 110957 https://doi.org/10.1016/j.fct.2019.110957.

Sohouli, E., Sadeghpour Karimi, M., Marzi Khosrowshahi, E., Rahimi-Nasrabadi, M., Ahmadi, F., 2020. Fabrication of an electrochemical mesalazine sensor based on ZIF-67. Meas. J. Int. Meas. Confed. 165, 108140. https://doi.org/10.1016/j.measurement.2020.108140.

Song, D., Jiang, X., Li, Yanshan, Lu, X., Luan, S., Wang, Y., Li, Yan, Gao, F., 2019. Metal−organic frameworks-derived MnO_2/Mn_3O_4 microcuboids with hierarchically ordered nanosheets and Ti3C2 MXene/Au NPs composites for electrochemical pesticide detection. J. Hazard. Mater. 373, 367–376. https://doi.org/10.1016/j.jhazmat.2019.03.083.

Sun, C., Wu, N., Kou, S., Wu, H., Liu, Y., Pei, A., Li, Q., 2023. Occurrence, formation mechanism, detection methods, and removal approaches for chloropropanols and their esters in food: An updated systematic review. Food Chem. X 17. https://doi.org/10.1016/j.fochx.2022.100529.

Tang, Y., Yang, G., Liu, X., Qin, L., Zhai, W., Fodjo, E.K., Shen, X., Wang, Y., Lou, X., Kong, C., 2023. Rapid sample enrichment, novel derivatization, and high sensitivity for determination of 3-chloropropane-1,2-diol in soy sauce via high-performance liquid chromatography-tandem mass spectrometry. J. Agric. Food Chem. 71, 15388–15397. https://doi.org/10.1021/acs.jafc.3c05230.

Teng, Y., Wang, X.D., Liao, J.F., Li, W.G., Chen, H.Y., Dong, Y.J., Kuang, D.Bin, 2018. Atomically Thin defect-rich Fe–Mn–O hybrid nanosheets as high efficient electrocatalyst for water oxidation. Adv. Funct. Mater. 28, 1–8. https://doi.org/10.1002/adfm.201802463.

Tran, L.T., Dang, H.T.M., Tran, H.V., Hoang, G.T.L., Huynh, C.D., 2023. MIL-88B(Fe)-NH_2: an amine-functionalized metal-organic framework for application in a sensitive electrochemical sensor for Cd^{2+}, Pb^{2+}, and Cu^{2+} ion detection. RSC Adv. 13, 21861–21872. https://doi.org/10.1039/d3ra02828c.

Tsai, H., Hsu, J., Fang, C., Su, N., 2021. Determination of glycidyl esters and 3-MCPD esters in edible oils by sample pretreatment with the combination of lipase hydrolysis and modified quechers for gc-ms analysis determination of glycidyl esters and 3-MCPD esters in edible oils by sample. J. Food Drug Anal. 29.

Wang, R., Xu, H., Zhang, K., Wei, S., Deyong, W., 2019. High-quality Al@Fe-MOF prepared using Fe-MOF as a micro-reactor to improve adsorption performance for selenite. J. Hazard. Mater. 364, 272–280. https://doi.org/10.1016/j.jhazmat.2018.10.030.

Xie, Q., Li, Y., Lv, Z., Zhou, H., Yang, X., Chen, J., Guo, H., 2017. Effective adsorption and removal of phosphate from aqueous solutions and eutrophic water by Fe-based MOFs of MIL-101. Sci. Rep. 7, 1–15. https://doi.org/10.1038/s41598-017-03526-x.

Xu, T., Qingru, Z., Fu, Q., Wang, Z., Liu, X., Xiao, S., Jiang, X., Lu, Y., Gong, Z., Wu, Y., Fang, M., 2023. Fluorescence determination of 3-MCPD by combining amino silica nanoparticles with fluorescein isothiocyanate. J. Anal. Sci. Technol. 14. https://doi.org/10.1186/s40543-023-00406-0.

Yaman, Y.T., Bolat, G., Saygin, T.B., Abaci, S., 2021. Molecularly imprinted label-free sensor platform for impedimetric detection of 3-monochloropropane-1,2−diol. Sens. Actuators, B Chem. https://doi.org/10.1016/j.snb.2020.128986.

Yang, A., Wang, Z., Zhu, Y., 2020. Facile preparation and adsorption performance of low-cost MOF@cotton fibre composite for uranium removal. Sci. Rep. 10, 1–10. https://doi.org/10.1038/s41598-020-76173-4.

Yang, Y., Lu, Z., Liu, D., Wang, Y., Chen, S., Li, T., 2021. A theoretical and simulation analysis of the sensitivity of sinws-fet sensors. Biosensors 11. https://doi.org/10.3390/bios11040121.

Yuan, Y., Wang, J., Ni, X., Cao, Y., 2019. A biosensor based on hemoglobin immobilized with magnetic molecularly imprinted nanoparticles and modified on a magnetic electrode for direct electrochemical determination of 3-chloro-1, 2-propandiol. J. Electroanal. Chem. 834, 233–240. https://doi.org/10.1016/j.jelechem.2018.12.034.

Zhao, Y., Xu, Y., Shi, L., Fan, Y., 2021. Perovskite nanomaterial-engineered multiplex-mode fluorescence sensing of edible oil quality. Anal. Chem. 93, 11033–11042. https://doi.org/10.1021/acs.analchem.1c02425.

Zheng, X., Fu, W., Zheng, K., Gao, B., Lin, L., Liu, W., Lin, Z., Fang, Q., 2020. A novel method for the simultaneous determination of esterified 2-/3-MCPD and glycidol in foods by GC-MS/MS. Food Control, 107766. https://doi.org/10.1016/j.foodcont.2020.107766.